

Observational insights on the origin of giant low surface brightness galaxies

Anna S. Saburova,^{1,2*} Igor V. Chilingarian,^{3,1} Anastasia V. Kasparova,¹
Olga K. Sil’chenko,¹ Kirill A. Grishin,^{1,4} Ivan Yu. Katkov,^{5,6,1} Roman I. Uklein⁷

¹ Sternberg Astronomical Institute, Moscow M.V. Lomonosov State University, Universitetskij pr., 13, Moscow 119234, Russia

² Institute of Astronomy, Russian Academy of Sciences, Pyatnitskaya st., 48, Moscow 119017, Russia

³ Center for Astrophysics — Harvard and Smithsonian, 60 Garden Street MS09, Cambridge, MA 02138, USA

⁴ Department of Physics, M.V. Lomonosov Moscow State University, 1 Vorobyovy Gory, Moscow 119991, Russia

⁵ New York University Abu Dhabi, PO Box 129188 Abu Dhabi, UAE

⁶ Center for Astro, Particle, and Planetary Physics, NYU Abu Dhabi, PO Box 129188, Abu Dhabi, UAE

⁷ Special Astrophysical Observatory, Russian Academy of Sciences, Nizhniy Arkhyz, Karachai-Cherkessian Republic 357147, Russia

5 March 2021

ABSTRACT

Giant low surface brightness galaxies (gLSBGs) with dynamically cold stellar discs reaching the radius of 130 kpc challenge currently considered galaxy formation mechanisms. We analyse new deep long-slit optical spectroscopic observations, archival optical images and published H α and optical spectroscopic data for a sample of seven gLSBGs, for which we performed mass modelling and estimated the parameters of dark matter haloes assuming the Burkert dark matter density profile. Our sample is not homogeneous by morphology, parameters of stellar populations and total mass, however, six of seven galaxies sit on the high-mass extension of the baryonic Tully–Fisher relation. In UGC 1382 we detected a global counterrotation of the stellar high surface brightness (HSB) disc with respect to the extended LSB disc. In UGC 1922 with signatures of a possible merger, the gas counterrotation is seen in the inner disc. Six galaxies host active galactic nuclei, three of which have the estimated black hole masses substantially below those expected for their (pseudo-)bulge properties suggesting poor merger histories. Overall, the morphology, internal dynamics, and low star formation efficiency in the outer discs indicate that the three formation scenarios shape gLSBGs: (i) a two-stage formation when an HSB galaxy is formed first and then grows an LSB disc by accreting gas from an external supply; (ii) an unusual shallow and extended dark matter halo; (iii) a major merger with fine-tuned orbital parameters and morphologies of the merging galaxies.

Key words: galaxies: kinematics and dynamics, galaxies: evolution, galaxies: formation

1 INTRODUCTION

Freeman (1970) discovered that the majority of galactic discs have exponential light profiles with nearly the same B -band central surface brightnesses of 21.65 mag arcsec⁻². However, over a decade later, deep photometric observations revealed the existence of fainter systems, which were named low surface brightness (LSB) galaxies. Bothun et al. (1987) discovered a separate subclass of a stellar system, giant LSB galaxies (gLSBGs) with a disc radius upto 130 kpc (Boissier et al. 2016) that is nearly ten times the radius of the Milky Way. These galaxies pose a problem in the currently accepted hierarchical galaxy formation paradigm. Despite they are among the most massive known galaxies reaching dynamical masses of 10^{12} and $\sim 10^{11} M_{\odot}$ in stars, they have large-scale dynamically cold discs.

It is very difficult to grow such high stellar mass in the hierarchical clustering paradigm without numerous major mergers (Rodríguez-Gomez et al. 2015) that would likely overheat and destroy the discs (Wilman et al. 2013). Most gLSBGs live in a sparse environment or total isolation (Saburova et al. 2018), and perhaps this can help to preserve gLSB discs through the cosmic time (Galaz et al. 2011; Pérez-Montaño & Cervantes Sodi 2019). However, at a certain stage of the gLSBGs evolution there should exist a large reservoir of gas sufficient to foster the formation of a massive gaseous disc.

The question ‘how do gLSBGs form?’ remains a matter of debate (see, e.g. Kasparova et al. 2014; Galaz et al. 2015; Boissier et al. 2016; Hagen et al. 2016; Saburova et al. 2018, and references therein). The recent studies discuss the two groups of gLSBGs formation scenarios, (i) non-catastrophic scenarios involving either slow gas accretion from filaments or secular evolution, and (ii) catastrophic models based on major- and/or minor-merger events.

* E-mail: saburovaann@gmail.com

The major advantage of catastrophic scenarios from the point of view of simulations is that they could work within the current galaxy formation framework. For example, [Zhu et al. \(2018\)](#) found an analogue of Malin 1 in the IllustrisTNG simulation, which satisfactorily reproduced most observed properties of Malin 1 and was formed by a merger of three quite massive galaxies. [Saburova et al. \(2018\)](#) considered a major-merger scenario among others in the case of UGC 1922, a gLSBG with a counterrotating inner gaseous disc. Using dedicated N-body/hydrodynamical simulations, they argued that its gLSB disc can be the result of an in-plane merger of a giant early-type spiral (Sa) galaxy and a gas-rich late-type (Sd) giant companion on a prograde orbit. However, the counterrotation observed in the central gaseous component with respect to the outer disc of UGC 1922 should be the result of another (minor) merger event. Despite relatively rich environment of UGC 1922 compared to other gLSBGs, [Saburova et al. \(2018\)](#) proposed that the major-merger scenario could also be a viable option for other galaxies of this class, which have fewer known companions.

Earlier, [Mapelli et al. \(2008\)](#) proposed another configuration of the catastrophic scenario that could lead to the formation of a gLSBG, a bygone head-on collision of a galaxy with a massive intruder, which could form a system similar to Malin 1 as a result of the expansion of a collisional ring. The weak point of this scenario is that the progenitor galaxy that experienced a collision should be already an LSB system. Also, [Kasparova et al. \(2014\)](#), [Boissier et al. \(2016\)](#) and [Hagen et al. \(2016\)](#) did not find evidence in favour of this scenario for Malin 2, Malin 1, and UGC 1382. Instead, to explain the origin of UGC 1382, [Hagen et al. \(2016\)](#) lean towards another widely discussed formation channel proposed by [Peñarrubia et al. \(2006\)](#), the accretion of several gas-rich low-mass satellites. Similar scenario is also proposed as one of the channels of the formation of massive discs by [Jackson et al. \(2020\)](#).

Despite the fact that most gLSBGs have diffuse clumps in their discs ([Kasparova et al. 2014](#); [Boissier et al. 2016](#); [Hagen et al. 2016](#); [Saburova et al. 2018](#)) which can be traces of recent mergers, the minor merger scenario by [Peñarrubia et al. \(2006\)](#) contradicts to most published H α gLSB observations (see, e.g. [Pickering et al. 1997](#); [Mishra et al. 2017](#)) because it predicts the fall-off of the rotational velocity at the periphery of the disc, which is not observed.

Along with the catastrophic formation scenarios for gLSBGs, several studies proposed non-catastrophic solutions, the scenarios which do not include a major merger or disruption of the satellites. [Noguchi \(2001\)](#) discussed the transformation of normal HSB spirals to gLSBGs through dynamical evolution due to a bar, which induces non-circular motions and radial mixing of disc matter that flattens the disc density profile. [Kasparova et al. \(2014\)](#) proposed that the large radius of the disc could be related to the a ‘sparse’ and shallow dark matter halo. They found that the dark matter halo of Malin 2 has the peculiarly high radial scale and low central density, and concluded that it could have caused the formation of a giant disc.

[Saburova \(2018\)](#) studied high surface brightness disc galaxies with slightly smaller (compared to gLSBGs) but still very large radii and highlighted a similar trend of larger radial scales of dark matter haloes for these systems in comparison to “normal-sized” disc galaxies. Central densities of dark matter haloes of HSB giant discs lie within the scatter for ordinary galaxies. Perhaps, to form a gLSBGs, both a large scale and a lower central density of the dark halo are required.

The evidence in favour of this idea were found e.g. in [Pérez-Montaño & Cervantes Sodi \(2019\)](#), who concluded that the spin parameters of LSB galaxies are systematically higher than those of HSB systems. If the baryons share the specific angular momentum

with a dark halo ([Fall & Efstathiou 1980](#)) than it could lead to larger radial scales of stellar discs and their lower baryonic surface densities in LSB galaxies, which was proved by self-consistent hydrodynamic simulations (see, e.g. [Kim & Lee 2013](#)). The properties of dark halos could, in turn, be related to the environment both at the stage of the galaxy formation and during its latter lifespan.

Most published works on gLSBGs are devoted to individual objects primarily because such objects are very difficult to observe and study in detail. In this paper we discuss a larger sample that includes seven gLSBGs. We present new observations for the four gLSBGs: Malin 2, NGC 7589, UGC 1382, and UGC 6614 and compare them to the data already available in the literature for Malin 1, UGC 1378, and UGC 1922. We present the results of long-slit spectral observations with the Russian 6-m telescope and the 8-m Gemini-North telescope. These data fill the central gap in low-resolution profiles of internal kinematics derived from radio observations in H α ([Pickering et al. 1997](#); [Mishra et al. 2017](#)) and give important clues about the central structure of gLSBGs. It allows us to build the most complete picture of the formation and evolution of these unusual systems up-to-date.

The paper is organized as follows. We describe our sample and properties of individual galaxies in Section 2. The details of observations and data reduction performed in this study are given in Section 3. We discuss the results of mass modelling of the rotation curves in Section 4 and give the details on it in Section 4.1. In Section 5, we discuss the star formation rates (SFRs) of gLSBGs, their position on the baryonic Tully–Fisher (TF) relation, and in Section 6 we discuss the properties of central regions of gLSBGs, propose the formation scenarios for each galaxy and compare gLSBGs with other extended LSB and giant HSB galaxies. Section 7 summarizes our findings.

2 OUR SAMPLE OF GIANT LOW SURFACE BRIGHTNESS GALAXIES

Our sample includes seven objects. To compare them against known high- and low-surface brightness galaxies, we display them in the size–luminosity diagram (see Fig. 1, coloured symbols) presenting a circularized effective radius¹ versus *V*-band absolute magnitude. In some cases we converted the available *g*-band fluxes and *g* – *r* colours into the *V* band using the transformations from [Jester et al. \(2005\)](#). We display bulges and gLSB discs separately. The former ones are shown with black outlines and darker colours. The black lines correspond to constant mean surface brightnesses. We also plot slightly smaller extended LSB galaxies (black squares, [Greco et al. 2018](#)); ultradiffuse galaxies (small crosses, [van Dokkum et al. 2015](#); [Chilingarian et al. 2019](#)), several families of early-type galaxies ([Brodie et al. 2011](#), small triangles); galaxies with morphological types later than 2 (i.e. discs) from the Hyperleđa data base (small circles). From the sample of [Greco et al. \(2018\)](#), we took only the objects with available spectroscopic redshifts.

From Fig. 1, it is evident that LSB discs of gLSBGs have similar mean surface brightnesses to LSBs extending their locus to higher luminosities and also for a given luminosity they are much more extended compared to ‘normal’ late-type galaxies from Hyperleđa. At the same time, bulges of gLSBGs are similar to those in HSB early- and late-type galaxies.

¹ We calculate a circularized effective radius following [Greco et al. \(2018\)](#) as $r_{\text{circ}} = (1 - \epsilon)^{1/2} r_{\text{eff}}$, where ϵ is an ellipticity and r_{eff} is a measured half-light radius.

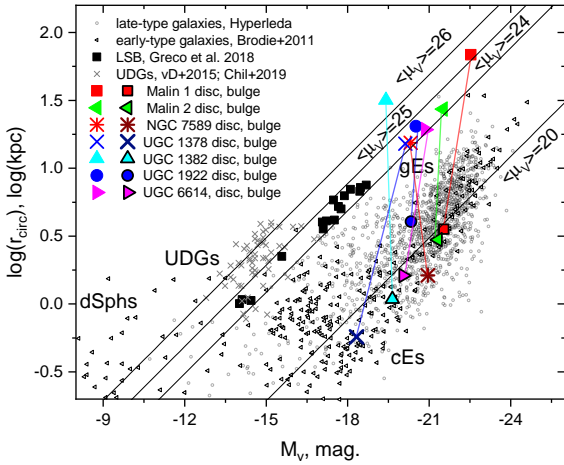


Figure 1. Position of gLSBG discs and bulges on the size-luminosity relation are shown by coloured and darker outlined symbols respectively. Bulge and disc positions of the same galaxy are connected by a line. Black squares show LSB galaxies from Greco et al. (2018) with spectroscopic redshifts. Small triangles display early-type galaxies from Brodie et al. (2011). Small circles correspond to late-type galaxies (with morphological type $t > 2$) from the Hyperleda database. Small crosses show ultradiffuse galaxies from van Dokkum et al. (2015) and Chilingarian et al. (2019). The solid diagonal lines show three values of a constant mean surface brightness.

We present the general properties of the gLSBGs from our sample in Tables 1 and 2. Below we briefly describe every individual system.

Malin 1 is the prototype of the gLSBG class discovered by Bothun et al. (1987). Similar to most gLSBGs, it has a prominent bulge and faint extended spiral arms. It shows signs of an active galactic nucleus (AGN) lying in the borderline of the LINER–Seyfert classification by emission-line ratios (Junais et al. 2020). Deep images of the galaxy revealed the well pronounced low surface brightness spiral arms (Galaz et al. 2015; Boissier et al. 2016) while the central part resembles a “normal” barred early-type spiral galaxy (SB0/a) with a bulge and an HSB disc (Barth 2007; Saha et al. 2021). Reshetnikov et al. (2010) presented spectroscopic evidence that Malin 1 is interacting with the small companion Malin 1B. They concluded that the interaction could lead to the appearance of a single dusty LSB spiral arm in Malin 1. The large-scale environment of Malin 1 is of low density. Based on multiband images of Malin 1, Boissier et al. (2016) conclude that its extended disc has been forming stars with a low star formation efficiency for several Gyrs.

Malin 2 is relatively well studied since its discovery by Bothun et al. (1990). It has a prominent bulge and a gLSBG disc with a spiral structure. According to Ramya et al. (2011) Malin 2 shows AGN activity. The estimated mass of the central black hole, $2.9 \times 10^5 M_{\odot}$ (Ramya et al. 2011) appears to be lower than expected for the observed stellar velocity dispersion. However, the $H\alpha$ line profile decomposition done using the technique presented in Chilingarian et al. (2018) does not reveal a broad-line component hence questioning the black hole mass estimate from Ramya et al. (2011). Das et al. (2010) revealed the presence of extended molecular gas in the disc of Malin 2 with the mass in the range from 4.9×10^8 to $8.3 \times 10^8 M_{\odot}$. The observed ratio of molecular to atomic hydrogen surface density is significantly higher than that expected in normal galaxies for the observed low value of the turbulent gas pressure and the total gas density. According to Kasparova et al. (2014), one possible explanation for this imbalance is the high content of unde-

tected cold gas (dark gas) in Malin 2. The fact that Malin 2 is bright in the NUV indicates the ongoing star formation in the system. The SFR estimate based on the NUV flux is $4.3 M_{\odot} \text{ yr}^{-1}$ (Boissier et al. 2008). Kasparova et al. (2014) also give the measurement of the SFR surface density in the disc of Malin 2 $\sim 2.5 \times 10^{-4} M_{\odot} \text{ yr}^{-1} \text{ kpc}^{-2}$ based on the archival GALEX data.

NGC 7589 was mentioned for the first time by Sprayberry et al. (1995). This galaxy has spiral arms, two bars and a ring. According to Lelli et al. (2010), NGC 7589 consists of an HSB central part and a gLSBG disc. The available $H\text{I}$ rotation curve exhibits a plateau at about 200 km s^{-1} from the radius of 5.9 kpc, there is no $H\text{I}$ data in the inner part (Lelli et al. 2010).

NGC 7589 is a Seyfert 1 galaxy with the mass of the central black hole estimated at $9.44 \times 10^6 M_{\odot}$ (Subramanian et al. 2016). The upper limit of the molecular hydrogen mass is $8.25 \times 10^8 M_{\odot}$ which corresponds to the low ratio of the molecular-to-atomic hydrogen of 0.081 (Cao et al. 2017). However, the global SFR is not very low: $1.00 M_{\odot} \text{ yr}^{-1}$ (deduced from the NUV flux, Cao et al. 2017) or 0.73 and $1.14 M_{\odot} \text{ yr}^{-1}$ (determined from far-ultraviolet (FUV) and near-ultraviolet (NUV) luminosities by Boissier et al. 2008).

UGC 1378 was classified as a gLSBG galaxy by Schombert (1998). Saburova et al. (2019) studied it in details using long-slit spectral observations and deep multiband optical photometry. Similarly to Malin 1 it has a complex morphology that includes a Milky way-sized central part with a bulge, bar and an HSB disc that is immersed in a large low surface brightness disc. The global SFR based on the infrared data is between 1.2 and $2.3 M_{\odot} \text{ yr}^{-1}$ (Saburova et al. 2019). At the same time, the SFR surface density of the LSB disc appears to be lower than expected for the given gas surface density, which can indicate the presence of accretion. No CO(1-0) emission was detected from the disc of this galaxy.

UGC 1382 had been misclassified as an elliptical galaxy before Hagen et al. (2016) noticed that it had an extended spiral structure visible in UV images obtained by Galaxy Evolution Explorer (GALEX, Martin et al. 2005). Further analysis of the multiwavelength data revealed that it appears to be a gLSBG with HSB bulge+disc surrounded by a gLSBG disc. The global SFR of UGC 1382 is $0.42 M_{\odot} \text{ yr}^{-1}$ and the SFR surface density of UGC 1382 is similar to that of the outer regions of spiral galaxies which is typical for low efficiency of star formation (Hagen et al. 2016). UGC 1382 lives in the low-density environment, at the same time Hagen et al. (2016) also discovered a possible remnant of a satellite embedded in its LSB disc.

UGC 1922 was erroneously classified as an elliptical galaxy too (see, e.g. Huchra et al. 2012). Schombert (1998) revealed the extended gLSBG disc in it. Saburova et al. (2018) performed deep long-slit and photometric observations of this galaxy and discovered the presence of a kinematically decoupled central component, which counter-rotates with respect to the main disc of the galaxy. The deep photometry of UGC 1922 revealed the asymmetric spiral structure with “rows” and irregular star formation on the NW-side. The disc appeared to be strongly dynamical overheated. Unlike many other gLSBG galaxies UGC 1922 is not isolated but a member of a group that includes seven members (Saulder et al. 2016).

UGC 6614 was initially studied by Schommer & Bothun (1983). It has a prominent bulge, spiral arms, and a ring. Like NGC 7589, it has an AGN and can be classified as LINER (Subramanian et al. 2016). The nucleus of UGC 6614 is bright in X-ray, optical and radio frequencies. The large amplitude, short time-scale of X-ray variability of UGC 6614 can be indication of active intense accretion onto the central black hole (Naik et al. 2010). The

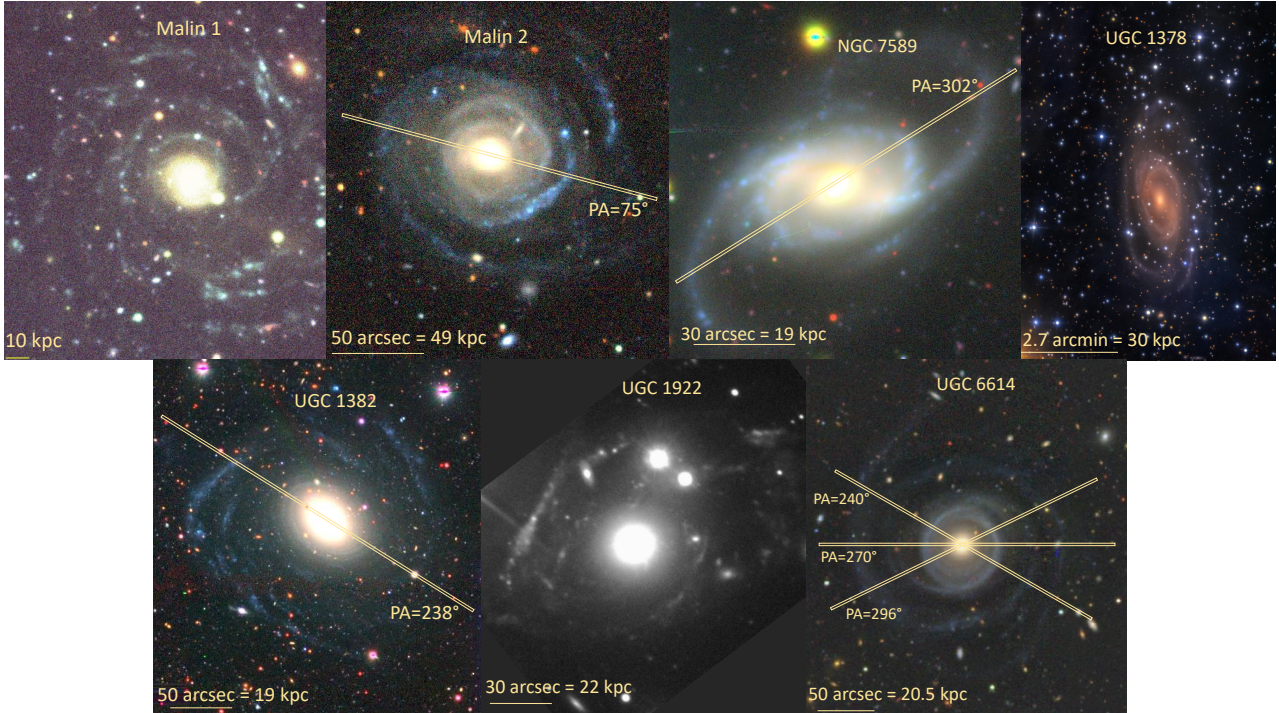


Figure 2. Direct images of the seven gLSBGs from this study. The slit positions are overplotted on the images of Malin 2, NGC 7589, UGC 1382, and UGC 6614. We used g, r, z images from DECaLS (Dey et al. 2019) for Malin 2 and UGC 6614 and from Subaru Hyper Suprime-Cam (Aihara et al. 2019) for NGC 7589 and UGC 1382. For Malin 1, we show a u, g, i -band image from the CFHT-Megacam Next Generation Virgo cluster Survey reproduced from Junais & Boissier (2019). For UGC 1378 we use a g, r, z -band image from the MMT Binospec from Saburova et al. (2019). For UGC 1922, we present a g -band image taken with 2.5-m telescope of the Caucasus Mountain Observatory, Sternberg Astronomical Institute from Saburova (2018).

estimate of the central black hole mass is $4.44 \times 10^6 M_{\odot}$, which appears to be lower than expected for observed stellar velocity dispersion similarly to that of Malin 2, that can indicate that it is not in co-evolution with the host galaxy bulge (Subramanian et al. 2016). The CO(1-0) emission was detected from the disc of UGC 6614 and the molecular gas traces its spiral arms (Das et al. 2006). The corresponding estimate of the mass of molecular gas in the disc is $2.8 \times 10^8 M_{\odot}$. The SFR determined from the infrared emission is $0.88 M_{\odot} \text{ yr}^{-1}$ (Rahman et al. 2007). We obtained the higher value of the global SFR based on GALEX FUV data and SFR vs UV-luminosity relation from Kennicutt (1998): $2.24 M_{\odot} \text{ yr}^{-1}$ and 1.44 for peripheral LSB regions. Our global SFR estimate is also higher than that derived by Wyder et al. (2009) from NUV data ($1.95 M_{\odot} \text{ yr}^{-1}$). The colour $FUV - NUV = 1.01$ mag of UGC 6614 is higher than what is usually observed in LSB galaxies according to Wyder et al. (2009). Together with a relatively low value of the SFR surface density of $2.14 \times 10^{-4} M_{\odot} \text{ yr}^{-1} \text{ kpc}^{-2}$ (Wyder et al. 2009), $3.17 \times 10^{-4} M_{\odot} \text{ yr}^{-1} \text{ kpc}^{-2}$ (current work), the red $FUV - NUV$ colour can indicate the absence of large amounts of stars younger than 10^8 yr. UGC 6614 contains a noticeable amount of dust: $2.6 \times 10^8 M_{\odot}$, the dust-to-gas mass ratio is 0.01 (Rahman et al. 2007) which is more than ten times higher than the typical value in spiral galaxies (Bettoni et al. 2003). Another interesting detail observed in UGC 6614 is the blueshifted ionized gas emission in $H\alpha$ that could indicate a jet or an accretion disc hot spot along the line of sight (Ramya et al. 2011).

Table 1. Equatorial coordinates (J2000.0) from NASA/IPAC Extragalactic Database (NED)^a for the gLSBGs from our sample.

Galaxy	RA	Dec
Malin 1	$12^{\text{h}} 36^{\text{m}} 59^{\text{s}}.350$	$+14^{\text{d}} 19^{\text{m}} 49^{\text{s}}.32$
Malin 2	$10^{\text{h}} 39^{\text{m}} 52^{\text{s}}.483$	$+20^{\text{d}} 50^{\text{m}} 49^{\text{s}}.36$
NGC 7589	$23^{\text{h}} 18^{\text{m}} 15^{\text{s}}.668$	$+00^{\text{d}} 15^{\text{m}} 40^{\text{s}}.19$
UGC 1378	$01^{\text{h}} 56^{\text{m}} 19^{\text{s}}.24$	$+73^{\text{d}} 16^{\text{m}} 58^{\text{s}}.0$
UGC 1382	$01^{\text{h}} 54^{\text{m}} 41^{\text{s}}.042$	$-00^{\text{d}} 08^{\text{m}} 36^{\text{s}}.03$
UGC 1922	$02^{\text{h}} 27^{\text{m}} 45^{\text{s}}.930$	$+28^{\text{d}} 12^{\text{m}} 31^{\text{s}}.83$
UGC 6614	$11^{\text{h}} 39^{\text{m}} 14^{\text{s}}.872$	$+17^{\text{d}} 08^{\text{m}} 37^{\text{s}}.21$

^a <https://ned.ipac.caltech.edu/>

3 SPECTROSCOPIC AND PHOTOMETRIC DATA

3.1 Spectroscopic observations and data reduction

3.1.1 Observations with the Russian 6-m telescope

Here, we present long-slit spectroscopic observations of four gLSBGs conducted with the SCORPIO universal spectrograph (Afanasiev & Moiseev 2005) at the prime focus of the Russian 6-m BTA telescope. We present the observing log in Table 3, which contains the position angle of the slit, date of observation, total integration time and the atmospheric seeing quality. We utilized the VPHG2300G volume phase holographic grism that yields the spectral resolving power of $R = 2400$ (full width at half-maximum $\sim 2.2 \text{ \AA}$) in the wavelength range $4800 < \lambda < 5570 \text{ \AA}$ sampled by $0.38 \text{ \AA pixel}^{-1}$. The plate scale along the 6-arcmin long, 1-arcsec-wide slit is $0.36 \text{ arcsec pixel}^{-1}$. In Fig. 2, we show direct images of gLSBGs included in our sample. For the four galaxies

Table 2. Basic properties of the sample of gLSBGs: name; radius of LSB disc (four disc radial scale lengths for all galaxies except Malin 1 for which we used the distance to the furthestmost measured points from the centre above the noise level and with an approximate exponential radial distribution of surface brightness; morphological type; mass of H α ; adopted distance; inclination angle to the line of sight; position angle; rotation velocity; radius of the B -band 25-mag isophote from HyperLeda^b; AGN activity flag: L=LINER, S=Seyfert; central black hole mass; global SFR.

Galaxy	R_{LSB} kpc	T	$M_{\text{H}\alpha}$ $10^{10} M_{\odot}$	D Mpc	i ($^{\circ}$)	PA ($^{\circ}$)	v (km s^{-1})	R_{25} (kpc)	AGN flag	M_{BH} $10^6 M_{\odot}$	SFR ($M_{\odot} \text{yr}^{-1}$)
Malin 1	130 ²	SBab ³	6.7 \pm 1.0 ⁴	377 \pm 8 ⁴	38 \pm 3 ⁴	10-60 ⁴	236 \pm 9.4 ⁵	11	L ¹³	3.63 ^{+0.84} _{-0.81} ¹³	1.2–2.5 ¹⁴
Malin 2	82 ⁶	Scd ³	3.6 \pm 0.4 ⁷	201 ⁸	38 \pm 3 ⁷	75 \pm 3 ⁷	320 \pm 7 ⁷	33	S2 ¹⁵	0.29 ^{+0.32} _{-0.20} ¹⁶	4.3 ¹⁴
NGC 7589	56 ⁴	SABa ³	1.5 \pm 0.3 ⁴	130 \pm 8 ⁴	58 \pm 3 ⁷	302 \pm 4 ⁷	205 \pm 3 ⁴	18	S ¹³	9.44 ^{+1.35} _{-1.24} ¹³	0.7–1.1 ¹⁴
UGC 1378	50 ⁹	SBa ³	1.2 \pm 0.2 ¹⁰	38.8 ¹⁰	59 \pm 5 ¹⁰	181 \pm 6 ¹⁰	282 \pm 11 ¹⁰	15	–	–	1.2–2.3 ⁹
UGC 1382	80 ¹¹	S0 ¹¹	1.7 \pm 0.1 ¹¹	80 ¹¹	46 ¹¹	58 ^c	280 \pm 20 ¹¹	13	L ¹⁹	–	0.42 ^{+0.30} _{-0.17} ¹¹
UGC 1922	84 ¹²	S? ¹	3.2 \pm 0.4 ¹⁰	150 ¹⁰	51 \pm 2 ¹⁰	128 \pm 3 ¹⁰	432 \pm 12 ¹⁰	18	L ¹⁶	0.39 ^{+0.18} _{-0.15} ¹⁶	2.2 ¹⁸
UGC 6614	54 ⁷	Sa ³	2.5 \pm 0.2 ⁷	85 ⁷	35 \pm 3 ⁷	296 \pm 3 ⁷	228 \pm 12 ⁷	16	L ¹³	4.44 ^{+0.63} _{-0.58} ¹³	0.9 ¹⁷ –2.24 ¹⁸

Reference – ¹ NED, ² Boissier et al. (2016), ³ HyperLeda, ⁴ Lelli et al. (2010), ⁵ Moore & Parker (2006), ⁶ Kasparova et al. (2014), ⁷ Pickering et al. (1997), ⁸ Das et al. (2010), ⁹ Saburova et al. (2019), ¹⁰ Mishra et al. (2017), ¹¹ Hagen et al. (2016), ¹² Saburova (2018), ¹³ Subramanian et al. (2016), ¹⁴ Boissier et al. (2008), ¹⁵ Schombert (1998), ¹⁶ Ramya et al. (2011), ¹⁷ Rahman et al. (2007), ¹⁸ current paper, ¹⁹ Chilingarian et al. (2017).

^b HyperLeda database (Makarov et al. 2014): <http://leda.univ-lyon1.fr/>

^c according to Fig. 3 in (Hagen et al. 2016)

with new long-slit observations presented here (Malin 2, UGC 6614, NGC 7589, and UGC 1382), we also overplot the slit positions.

The spectroscopic data reduction for SCORPIO using our IDL-based pipeline is described in details in Saburova et al. (2018). It includes a bias subtraction and overscan clipping, flat-field correction, the wavelength calibration using arc lines², cosmic-ray hit removal, linearization, co-adding; the night sky subtraction using the algorithm described in Katkov & Chilingarian (2011) and flux calibration using the spectrophotometric standard stars *Feige 34*, *BD 33+2642*, *Feige 110*.

We took into account the instrumental line-spread function of the spectrograph along the slit and across the wavelength range, which we determined by fitting the twilight sky spectrum observed during the same night with an $R = 10000$ Solar spectrum using the PPFX full spectrum fitting technique (Cappellari & Emsellem 2004). We then fitted the galaxy spectra using intermediate-resolution ($R = 10000$) PEGASE.HR (Le Borgne et al. 2004) simple stellar population (SSP) models computed for the Salpeter initial mass function (IMF) (Salpeter 1955) convolved with the instrumental line-spread function of SCORPIO using the NBURSTS full spectral fitting technique (Chilingarian et al. 2007a,b). As the result of the procedure, we obtained the best-fitting parameters of an SSP model, that is age T (Gyr) and metallicity [Fe/H] (dex) of stellar population. The line-of-sight velocity distribution (LOSVD) of stars was parametrized by the Gauss–Hermite function until the fourth order (see van der Marel & Franx 1993). The resulting LOSVDs are characterized by the line-of-sight velocity, velocity dispersion and Gauss–Hermite moments h_3 and h_4 , which reflect the deviation of an LOSVD from the pure Gaussian profile.

We also analyzed the emission spectra which we obtained by subtracting the best-fitting stellar population templates from observed spectra. We fitted emission lines by a single Gaussian profile

Table 3. Observing log for SCORPIO.

Galaxy	Slit PA ($^{\circ}$)	Date	Exposure time (s)	Seeing (arcsec)
Malin 2	75	13.03.2018	10800	1.3
NGC 7589	302	21.09.2017	7200	1.4
UGC 1382	238	07.10.2016	7200	1.5
UGC 6614	296	15.03.2018	9000	2.0

and derived the velocity and velocity dispersion of ionized gas also taking into account the instrumental line spread function.

3.1.2 Gemini-North observations

For UGC 6614 we also found deep spectroscopic data in the Gemini science archive³. The galaxy was observed in the two different programs with the GMOS-N spectrograph operated at the 8-m Gemini-North telescope (programs GN-2006B-Q-41, P.I.: C. Onken and GN-2005B-Q-61, P.I.: L. Ferrarese). The details of GMOS-N observations are given in Table 4 where we list the position angles of the slit, the dates of observation, total integration time, slit widths, gratings, wavelength range, and spectral resolution for each data set.

We used our own IDL-based data reduction pipeline for GMOS data presented in (Francis et al. 2012). The data reduction for the GMOS-N observations obtained in the framework of the program GN-2006B-Q-41 was identical to those for Malin 2 presented in Kasparova et al. (2014). Data reduction for intermediate-resolution B1200 data from the program GN-2005B-Q-61 was done in a similar fashion. We updated our data reduction pipeline to handle low-resolution R400 grating data, which turned out to be very useful for tracing faint H α emission in the LSB disc of UGC 6614. Unfortunately, because of the chip gaps in GMOS-N and slightly different wavelength ranges used in the two programs, the B1200 dataset

² To improve the wavelength solution accuracy we took arc spectra every 2 h and used them to reduce the corresponding science frames.

³ <http://archive.gemini.edu/>

from GN-2006B-Q-41 had $H\beta$ missing, and the B1200 data set from GN-2005B-Q-61 had $[O\text{III}]$ missing.

We analysed the GMOS-N data using `NBURSTS` in a similar way to the SCORPIO observations described above.

3.2 Results of the analysis of spectroscopic data.

In Fig. 3, we demonstrate the main results of the analysis of spectral data for Malin 2. The left-hand column corresponds to the profiles of velocity and velocity dispersion for ionized gas (shaded lines) and stars (circles). The central column shows age and metallicity of stellar population. The right-hand column gives the profiles of h_3 and h_4 for the stellar LOSVD. The stars do not show clear rotation in the inner region.

The trend of stellar metallicity is very close to that found by Kasparova et al. (2014) – the decreasing radial gradient from almost solar metallicity in the centre. The age of stellar population is very old in the bulge region. The values of h_3 and h_4 are close to zero.

In Fig. 4, we demonstrate the results of our data analysis for NGC 7589. The designations are the same as in Fig. 3. As one can see in Fig. 4, the kinematics of the ionized gas of NGC 7589 is very complex: The velocity dispersion measured from the line $[O\text{III}]$ rises with the distance from the centre, which is not seen in $H\beta$. It leads to a lower velocity and a shallower velocity gradient for $[O\text{III}]$ in comparison to those derived from $H\beta$. This likely happens due to the presence of an AGN in NGC 7589 (see Sect. 2). The stellar age appears to be younger for the innermost part in comparison to that at larger radii. It and the non-zero values of h_3 and h_4 could be an indirect indication for the nuclear disc in the galaxy.

In Fig. 5, we present the results for UGC 1382. The gaseous component counter rotates with respect to the stars at all radii. The ionized gas is corotating with the extended $H\text{I}$ disc if we compare our profile with the $H\text{I}$ velocity map presented in Hagen et al. (2016). The stars in the centre are very old and show the considerable increase of metallicity. The age of stellar population of HSB part of the galaxy that we obtained in the current paper is significantly higher than that derived by Hagen et al. (2016) from SED fitting that is likely caused by the presence of a small fraction of young stars that strongly affect the blue part of the SED. The h_3 value is close to zero, at the same time h_4 is roughly 0.1 which could indicate the presence of a kinematically decoupled stellar component.

Fig. 6 shows the kinematics and stellar population profiles for GMOS-N and SCORPIO observations of UGC 6614. The kinematics in the inner region of UGC 6614 is also very complex. The motion of the ionized gas is different from that of the stellar population. In the innermost region ($R \leq 5$ arcsec), the ionized gas does not rotate or even shows signs of counterrotation. In contrast to UGC 1922, the inverted velocities are visible here only for one position angle $PA = 296^\circ$ and are concentrated in the innermost region unlike in UGC 1382 where the counterrotation of the gas is global. Hence, probably this feature traces the AGN-driven gas outflow noticed by Ramya et al. (2011) rather than a kinematically decoupled nuclear component. However, a high-resolution two-dimensional velocity field is needed to draw firm conclusion. The velocity dispersion measured from the $[O\text{III}]$ line differs from that of $H\beta$, similarly to NGC 7589, where the AGN also can affect the kinematics.

Another peculiarity of the ionized gas LOS velocity profile is a drop of the velocity on both sides from the centre at the radius of ~ 30 arcsec, in the vicinity of the inner bright ring of the galaxy. This drop manifests itself also in the velocity profile of stars. The change of the gradient of the velocity is similar to that often observed

in galaxies with bars (see, e.g. Saburova et al. 2017, and references therein). It is possible that the ring we see in UGC 6614 is a resonant ring. It could be oval, elliptical ring in which elliptical streamlines occur and non-circular motions show themselves in the decrease of the LOS velocity. Possibly, there was a weak bar in UGC 6614 before, which aided in accumulation of the material in the ring.

McGaugh et al. (2001) also obtained ionized gas LOS velocity profile of UGC 6614 in the $H\alpha$ line from the long-slit observations at $PA = 108^\circ$. In the inner region of their profiles, one can see the hint of the change of the velocity gradient. The rotation curve obtained in current paper is in a good agreement with their data – showing rotation velocity amplitude of ~ 200 km s^{-1} and the minimum at 10 kpc (see Fig. 6).

The stellar population of the bulge of UGC 6614 is old and metal-rich. The age of stars decreases with the distance from the centre and appears to be about 2–3 Gyr outside the region where the bulge dominates the luminosity. The metallicity of stars in this radius is roughly -0.5 dex. The values of h_3 and h_4 are non-zero, in particular h_3 anticorrelates with the velocity and h_4 has a minimum in centre, which is usually observed in barred galaxies (see, e.g. Saburova et al. 2017, and references therein).

3.3 Surface photometry of NGC 7589 and UGC 6614

To estimate the structural parameters of NGC 7589 and UGC 6614, we performed their surface photometry. We took publicly available data from the Subaru HyperSuprimeCam Strategic Survey DR2 for NGC 7589 and Zwicky Transient Facility (ZTF) (Bellm et al. 2019) survey for UGC 6614, both in the r band. We performed the isophote analysis using the `ELLIPSE` task in the `PHOTUTILS PYTHON` library. Then we found a multicomponent best-fitting model by minimizing χ^2 statistics for several light profiles. During this procedure, we convolve our model with a PSF, which we derived by fitting unsaturated stars in the same image.

NGC 7589 has a complex morphology in the centre which includes two bars and a ring. We excluded the central 17 arcsec from our analysis and fitted only the outer part of the light profile by a Sersic component and an exponential disc. As we show below, the masking of the central part of the profile has little effect on the DM halo parameters (that is the main goal of the approach).

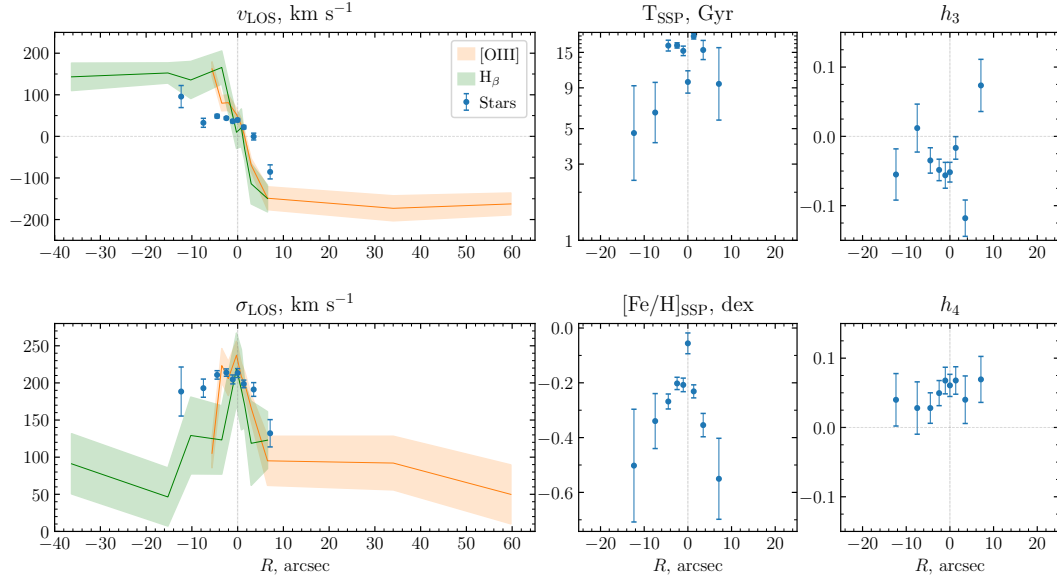
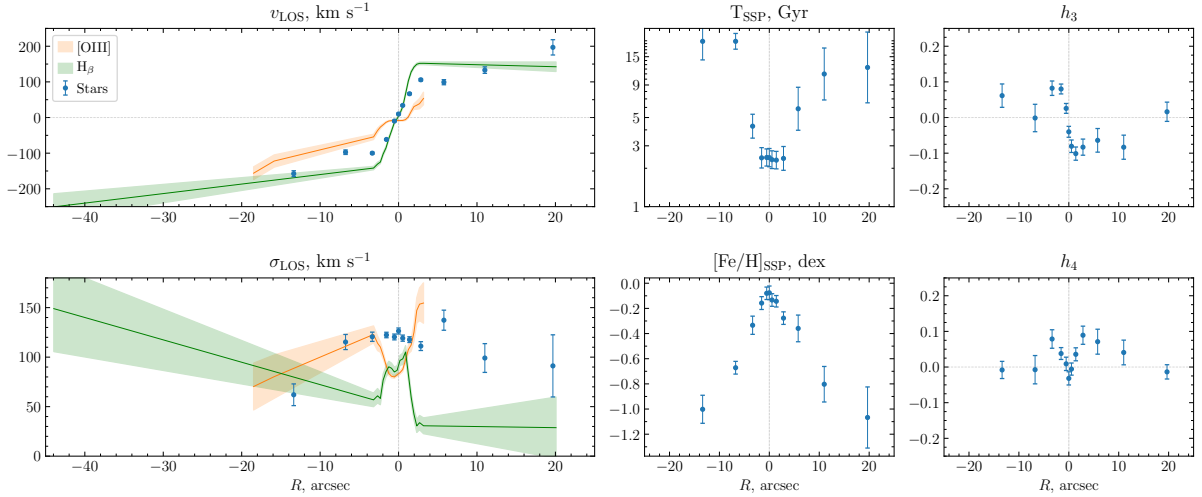
UGC 6614 spans two adjacent fields in ZTF, hence we added them into one mosaic using the `SWARP` software (Bertin 2010). Unlike ZTF-images, images in other surveys like SDSS or Legacy Survey, where spatial resolution is significantly better, have artefacts near bright objects which are usually caused by the local sky background subtraction algorithm. In case of UGC 6614 these artefacts prevent a precise light profile decomposition that includes an LSB disc, that is why we decided to use much shallower ZTF data unaffected by sky oversubtraction. We fitted the profile of UGC 6614 by two Sersic components. A one-dimensional multicomponent light profile decomposition is known to be unstable with respect to the additive background in the original image and also requires a rather fine-tuned initial guess (see e.g. Chilingarian et al. 2009b), therefore it is crucial to use data with a precisely subtracted sky background.

We demonstrate the results of the decomposition of the profiles into inner and LSB disc components for NGC 7589 and UGC 6614 in Figs. 7 and 8. The parameters of LSB discs and inner components are provided in Table 5 for both galaxies.⁴

⁴ We also attempted to use a model with a Sersic inner component and an outer exponential disc for UGC 6614, but the model with two Sersic

Table 4. Observing log for UGC 6614 (GMOS-N)

Program ID	Slit PA ($^{\circ}$)	Date	Exposure time (s)	Slit width (arcsec)	Grating	Wavelength range \AA	Spectral resolution
GN-2006B-Q-41	240	24.01.2007	5400	0.5	B1200+G5301	4672–6071	3400
GN-2005B-Q-61	270	26.12.2005	13200	0.75	B1200+G5301	4476–5800	2800
GN-2005B-Q-61	270	29.11.2005	4800	0.75	R400+G5305	3900–7864	800


Figure 3. Analysis of spectral observations of Malin 2. Left-hand panel: radial profile of the line-of-sight velocity v (upper panel) and velocity dispersion σ (bottom panel) of ionized gas (lines with shaded uncertainty areas) and stars (circles). Centre panel: radial profiles of stellar age (top panel) and metallicity (bottom panel). Right-hand panel: radial profiles of h_3 (top panel) and h_4 (bottom panel).

Figure 4. Analysis of spectral observations of NGC 7589. The designations are the same as in Fig. 3.

components yielded better fitting quality. The deviation of the model profile from the observed data at large radii does not affect the subsequent analysis because (i) we used a non-parametric description of the outer disc component as a difference between the total and bulge profiles in the rotation curve decomposition for UGC 6614 and (ii) a radial velocity profile does not reach the outermost part of the disc where the deviations are significant.

4 DYNAMICAL MODELLING USING THE ROTATION CURVE DECOMPOSITION

The dark matter halo is known to play an important role in galaxy evolution. Here, we derive the parameters of dark matter haloes in gLSBGs to compare them to HSB galaxies. In the previous studies of gLSBGs, Pickering et al. (1997); de Blok et al. (2001); Hagen et al. (2016); Lelli et al. (2010); Junais et al. (2020); Di Paolo et al.

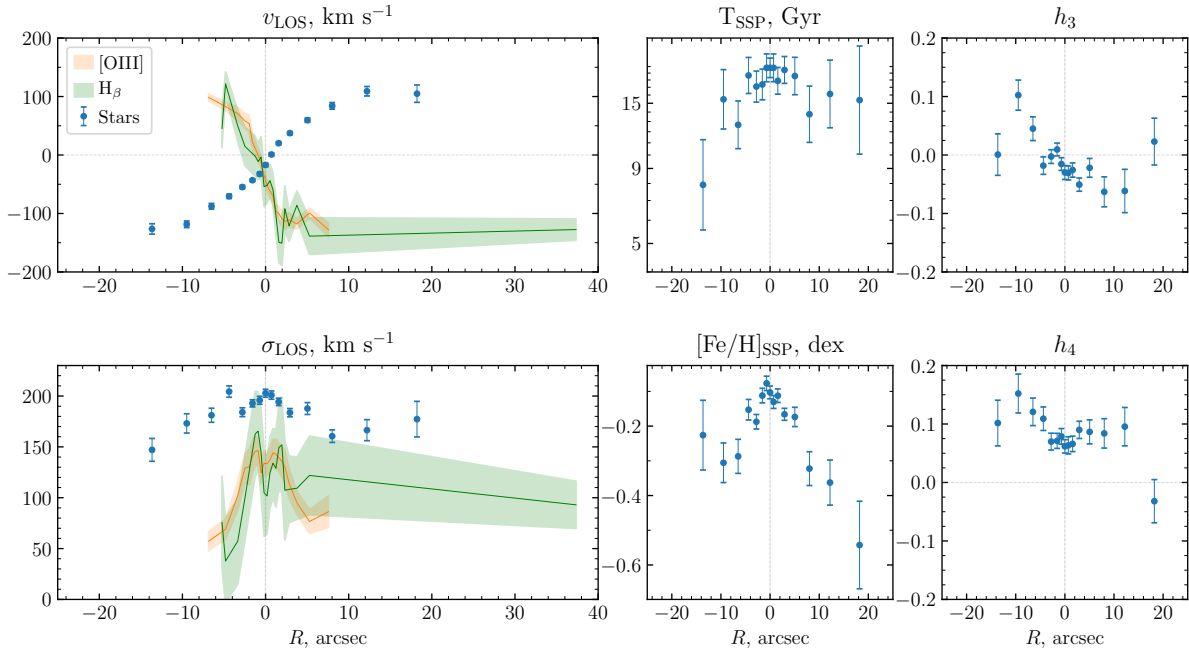


Figure 5. Analysis of spectral observations of UGC 1382. The designations are the same as in Fig. 3.

Table 5. The parameters of the r -band decomposition of the surface brightness profiles of NGC 7589 and UGC 6614. For UGC 6614, the disc was modelled by a Sersic profile, for NGC 7589, we used a pure exponential disc. The columns are (1) galaxy name; (2) total magnitude of the Sersic inner component; (3) effective radius of the Sersic inner component; (4) Sersic index of the inner component; (5)–(7) the same as (2)–(4) but for the outer disc component.

Galaxy	m_{in} mag	$(R_e)_{in}$ arcsec	n_{in}	m_d mag	$(R_e)_d$ arcsec	n_d
NGC 7589	13.41 ± 0.05	12.03 ± 0.17	0.57 ± 0.02	14.33 ± 0.09	47.74 ± 2.23	1
UGC 6614	13.88 ± 0.03	4.35 ± 0.08	1.52 ± 0.02	13.03 ± 0.08	51.63 ± 2.20	0.93 ± 0.11

(2019) also performed mass modelling using different profiles of dark matter halo (Einasto, NFW, Burkert and pseudo-isothermal) for different galaxies, hence no direct comparison of the objects is possible. Therefore, here we perform the rotation curve decomposition using the same dark matter halo profile for all galaxies in our sample. We combine the optical data presented in this paper with the published H α data, and then decompose the rotation curves for Malin 2, NGC 7589, UGC 1382, and UGC 6614. We derived the optical rotation curves from the H β and [O III] emission lines corrected for the systemic velocity, symmetrically reflected about the galaxy centre and de-projected using the inclination angle provided in Table 2.⁵

In the decomposition procedure, we included the following components: a stellar disc, a bulge, an H α disc, and a Burkert (1995) dark matter halo.⁶ We used the gas surface densities from published H α observations. The details of the procedure of mass-modelling are described in Saburova et al. (2016a). We give the specifications of the mass-modelling and the models for each galaxy in Section 4.1.

We fixed the contributions of stellar components according to the colour and spectral information. We also performed a decompo-

sition of the combined rotation curve of Malin 1 using the published data. The results of mass-modelling for UGC 1378 and UGC 1922 are taken from Saburova et al. (2018, 2019).

In Fig. 9, we plot the parameters of dark matter haloes against the 25 mag B -band isophote of gLSBGs and the sizes of gLSBG discs from Table 2. We also plot the parameters of intermediate-size and giant HSB galaxies from Saburova (2018) (black dots and triangles). The solid lines show the running median for HSB galaxies. From Fig. 9, it is evident that gLSBGs behave differently from HSB galaxies, some of them lie on the continuation of the best-fitting relation for HSB galaxies, but some deviate from it. This could suggest different nature and formation scenarios for different gLSBGs in our sample.

For NGC 7589, Malin 2, UGC 6614, and UGC 1922⁷, the parameters of the dark haloes agree better with the radius of the gLSBG disc than with R_{25} . The three remaining gLSBGs lie close to HSB galaxies in the diagrams for optical radius. This could indicate that the parameters of dark haloes of some of gLSBGs are connected to the sizes of their HSB parts, which can favour the two-stage formation of these systems. At first, the HSB part is formed, then a build-up of an extended LSB part occurs. Interestingly, the HSB-part of Malin 2 is also very extended.

⁵ For UGC 6614 three cuts are not along major axis, which was taken into account, see below.

⁶ We chose Burkert profile to compare with the sample of giant HSB galaxies where it was used by Saburova (2018).

⁷ It is worth noting, the uncertainty in the halo parameters does not draw the clear conclusion in the cases of NGC 7589 and UGC 1922.

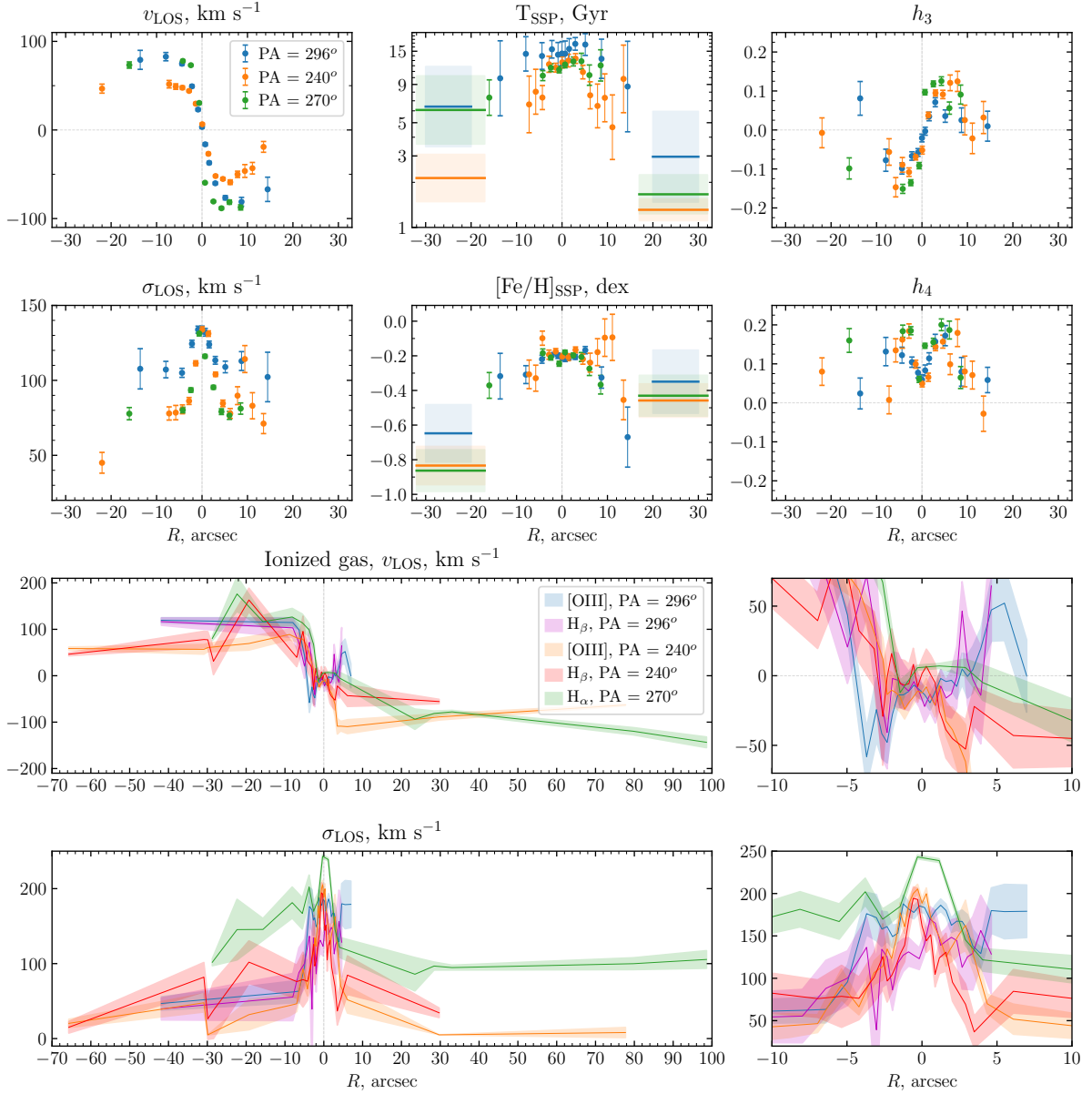


Figure 6. Analysis of spectral observations of UGC 6614 for three different position angles obtained at BTA and Gemini. Top two rows, left-hand panel: stellar kinematics, v (top panel) and σ (bottom panel); centre panel: stellar populations, age (top panel) and metallicity (bottom panel); right-hand panel: LOSVD deviation from the Gaussian shape, h_3 (top) and h_4 (bottom panel). Two bottom rows: v (top panel) and σ (bottom panel) of ionized gas for different PA and emission lines (see the legend). Left- and right-hand panels demonstrate full radial profiles and their zoomed central regions correspondingly.

Table 6. The parameters of the main structural components of the galaxies with 1σ uncertainties. The columns contain the following data: (1) galaxy name; (2) and (3) – radial scale and central density of the DM halo; (4) mass of the DM halo inside the LSB disc radius given in Table 2; (5) central surface density of the bulge; and (6) disc mass.

Galaxy	R_s	ρ_0	M_{halo}	$(I_0)_b$	M_{disc}
	kpc	$10^{-3} M_{\odot}/\text{pc}^3$	$10^{10} M_{\odot}$	$10^3 M_{\odot}/\text{pc}^2$	$10^{10} M_{\odot}$
Malin 1	19.6 +6.4 -5.8	6.6 +5.7 -2.5	78.3 +13.2 -15.1	25.2	13
Malin 2	52.2 +8.2 -4.8	3.3 +0.5 -0.6	164.4 +3.8 -4.1	6.4	31
NGC 7589	19.6 +7.6 -4.1	5.9 +2.4 -2.4	34.3 +4.3 -3.9	–	1.2
UGC 1382	16.3 +1.6 -2.1	28.6 +9.3 -5.3	157.2 +4.1 -8.7	9.2	5.7
UGC 6614	32.5 +7.7 -4.6	4.5 +1.0 -1.0	59.3 +6.4 -5.0	13.0	1.5

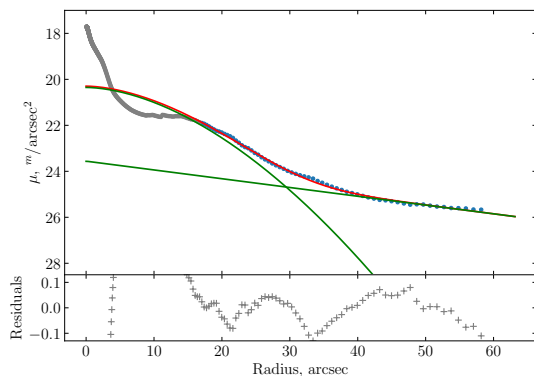


Figure 7. The results of the decomposition of the HSC r -band surface brightness profile of NGC 7589 into Sersic and exponential disc components. The central part inside the 17-arcsec ring is excluded from the analysis and greyed out.

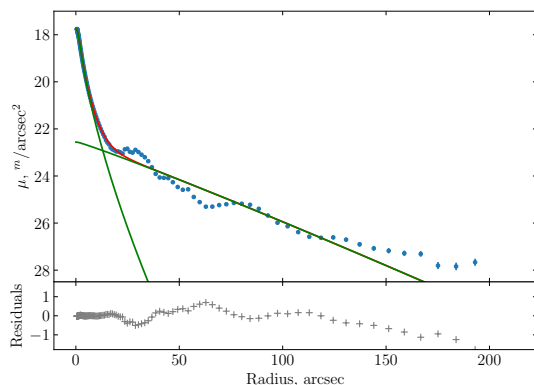


Figure 8. The results of the decomposition of the r -band surface brightness profile of UGC 6614 into two Sersic components.

4.1 Details on the fitting of rotation curves for individual galaxies

For Malin 1, we utilized the combined optical and H α rotation curve and surface density profile plus the R -band surface brightness profile from Lelli et al. (2010). We took optical the major axis rotation curve from Junais et al. (2020).⁸ We used a non-parametric definition of the contribution of the disc to the rotation curve. For this, we obtained the bulge parameters from the fitting of the light brightness using a Levenberg–Marquardt non-linear least-squares minimization routine in IDL (Chilingarian et al. 2009b). We fix R -band mass-to-light ratios to 3.0 for the disc and limited it to the range 2, . . . , 6 for the bulge, which correspond to the densities in agreement with those found by Boissier et al. (2016). We present the results of the rotation curve fitting in Fig. 10.

Our estimate of the dark halo radial scale appears to be higher than that obtained by Lelli et al. (2010) but within the range given by Junais et al. (2020) even keeping in mind that they used pseudo-isothermal dark matter profiles rather than the Burkert profile.

For Malin 2, we constructed a combined ionized gas (current paper) and H α rotation curve (Pickering et al. 1997). We use the parameters of the bulge obtained in g band from the light profile

⁸ We decided to use only the major axis since it was taken with the narrowest slit to avoid possible biases due to a non-homogeneous illumination of the slit and also to minimize the uncertainty because of poorly known orientation of the disc.

published in Kasparova et al. (2014) (Sersic index $n = 0.89 \pm 0.00$, central surface brightness $\mu_0 = 18.47 \pm 0.06$ mag arcsec⁻², effective radius $R_e = 1.10 \pm 0.05$ arcsec), and a non-parametric definition of the surface density profile of the disc. The disc g -band mass-to-light ratio was limited in the range 1.98, . . . , 3.89 according to the SED fitting (lower value) and the criterion of the marginal gravitational stability of the disc applied to the stellar velocity dispersion data at $r = 20$ arcsec from Kasparova et al. (2014) in a similar way as it was done for UGC 1378 (see Saburova et al. 2019).

The value following from the marginal gravitational stability is about twice as high as that resulting from the spectral and SED fitting obtained in Kasparova et al. (2014), which can indicate the mild overheating of the disc, especially if one takes into account the uncertainty because of the stellar IMF. The bulge mass-to-light ratio was limited to 3.33, . . . , 5.0 according to Kasparova et al. (2014). The results of the decomposition are shown in Fig. 11. One can see that for Malin 2, the model of its rotation curve rises too steep compared to observations. The probable reason of this discrepancy is the resolution of the spectral data that could smooth the steep rise of the rotation curve in the inner 2 kpc where the inconsistency is observed (the seeing quality corresponded to the resolution 1.3 kpc).

The radial scale of dark matter halo appears to be in good agreement with that found by Kasparova et al. (2014) if one applies the transformation coefficient from a pseudo-isothermal to Burkert dark halo profiles from Boyarsky et al. (2009). The core radius found by Di Paolo et al. (2019) is higher than that found in the current paper.

For NGC 7589, we performed the decomposition of the r -band light profile obtained from the SUBARU HSC data (Aihara et al. 2019). The surface brightness profile shows complex behaviour in the inner part due to the presence of two bars, a nuclear mini-bar with the radius of 2.5 arcsec and the ‘normal’ large-scale bar with the radius of 15 arcsec. Because of this, we calculated the contribution of the inner component to the rotation curve only approximately by considering it as the point mass $V^2 = GM/R$ and masked out the inner part of the rotation curve during the fitting. The mass M was estimated from the r -band luminosity in the aperture with the radius of 17 arcsec without the contribution of the LSB disc ($1.7 \times 10^{10} L_\odot$). The H α data are taken from Lelli et al. (2010). The inner rotation curve was derived in this paper from the ionized gas (H β) kinematics. The mass-to-light ratio of the inner component was limited in the range 1.4, . . . , 2.8 during the fitting. The lower value corresponds to the stellar population with the age of 4 Gyr and solar metallicity (see Fig. 4) for the Kroupa IMF. The upper value comes from the bulge colour $g - r = 0.76$ obtained from the SDSS images and the Roediger & Courteau (2015) model M/L -colour relations. For the disc, we considered the M/L_r in the range 1.3 . . . 2 according to its colour $g - r = 0.56$ estimated from the SDSS images and model relations from Roediger & Courteau (2015) and Bell et al. (2003). The result of the rotation curve modelling for NGC 7589 is shown in Fig. 12. The fact that we masked out the inner part of the rotation curve makes the model results more uncertain. This leads to the uncertainties of dark halo parameters of 50 per cent (see, Saburova et al. 2016b).

The dark halo radial scale is lower than that found by Di Paolo et al. (2019) but is in good agreement with that obtained by Lelli et al. (2010) for a pseudo-isothermal dark halo, however, they maximized the contribution of the stellar component, which we did not do here.

For UGC 1382, the ionized gas is co-rotating with the H α disc, which allowed us to build the combined rotation curve. We took the H α data from Hagen et al. (2016), the structural parameters of the bulge from Hagen et al. (2016), and a non-parametric definition

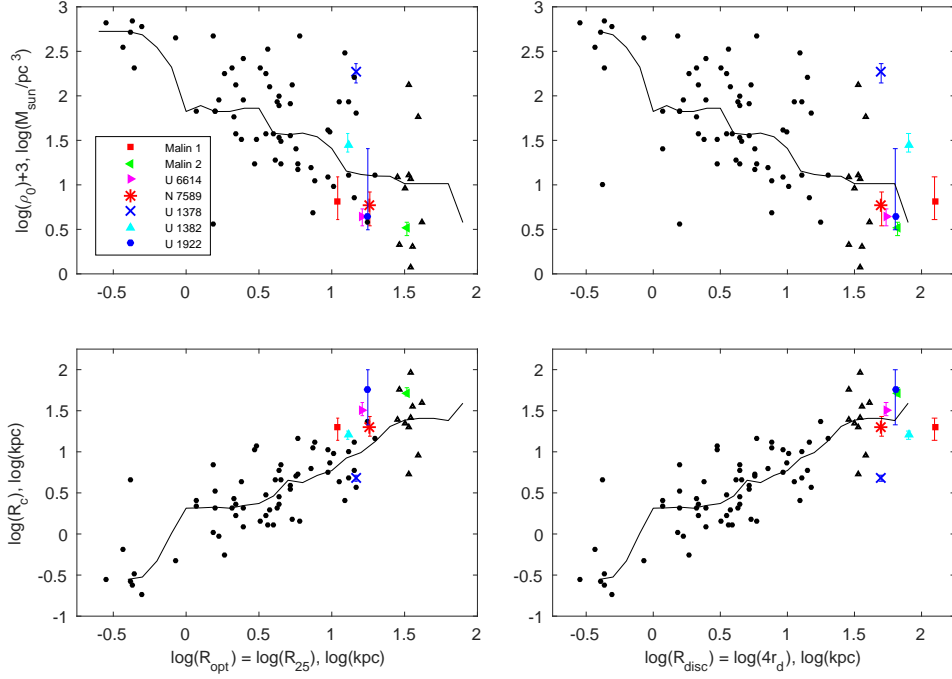


Figure 9. Left-hand panel: the optical radius (R_{25}) compared to the parameters of dark matter halo, central density (top panel) and radial scale (bottom panel). Right-hand panel: the same but for the disc radii from Table 2 for gLSB and R_{25} for HSB galaxies. The gLSBGs are shown by coloured symbols. Black triangles correspond to the giant HSB galaxies from Saburova (2018), black dots are for galaxies of moderate size, the solid lines are the running medians for non-LSB galaxies.

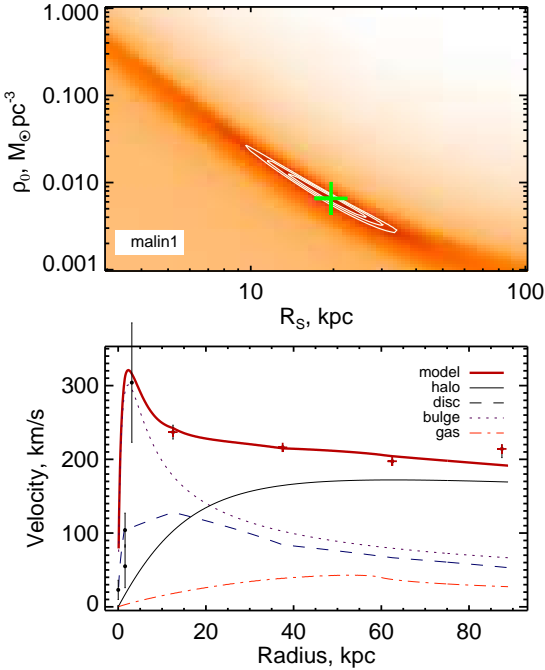


Figure 10. The results of the rotation curve decomposition for Malin 1: χ^2 map for the parameters of Burkert dark matter halo (top panel) and the fit of the rotation curve (bottom panel). Black dots on the rotation curve correspond to the data from Junais et al. (2020) taken along major axis. Red symbols show H α data.

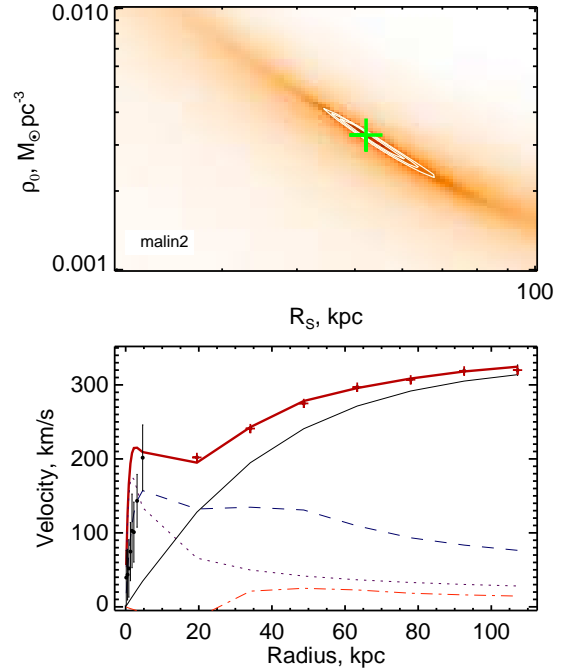


Figure 11. The results of the rotation curve decomposition for Malin 2. χ^2 map for the parameters of Burkert dark matter halo (top panel) and the fitting of the rotation curve (bottom panel). Black and red symbols on the rotation curve correspond to optical and H α data respectively.

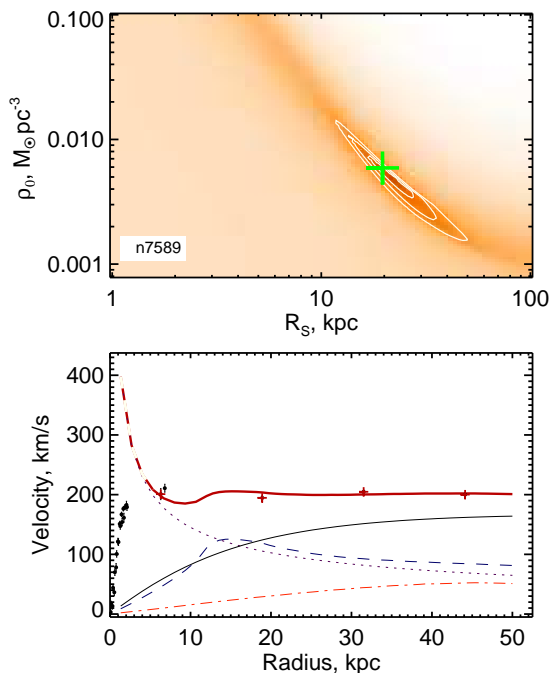


Figure 12. The results of the rotation curve decomposition for NGC 7589. The designations are the same as in Fig. 11. Central part of the rotation curve was masked-out during the fitting.

of the disc surface density profile – we obtained it as a difference between the total and a bulge r -band surface brightness profiles. The r -band mass-to-light ratio of the bulge was limited in the range 3. . . ,5 according to the stellar metallicity -0.1 and old age 13 Gyr for Kroupa (2001) and Salpeter (1955) stellar IMF (see Fig. 5). For the disc the limits 1.2. . . ,2.66 come from the relation by Roediger & Courteau (2015) and the $g - r$ colour of the disc and from Hagen et al. (2016). We present the results of modelling in Fig. 13. Hagen et al. (2016) also performed the mass modelling of the rotation curve of UGC 1382, however, they used the Einasto and NFW dark halo density profiles. Their model shows a similar behaviour to ours, the baryonic contribution to the rotation curve dominates only in the inner 10 kpc, while the dark halo dominates at larger radii.

For UGC 6614 due to the complex gas kinematics in the inner region we excluded the innermost points ($R \leq 1.6$ kpc) from our analysis. We calculated the ionized gas rotation curve from the two spectral cuts ($PA = 240, 270^\circ$) based on the measurements in $H\alpha$ and $[OIII]$ emission lines. We estimated the circular velocity from the observed line-of-sight velocity and the radial coordinate R taking into account inclination of the disc and the angle between the radius-vector of a given point and the major axis of a galaxy ϕ : $V(R) = \frac{V_r(R) \sqrt{(\sec^2(i) - \tan^2(i) \cos^2(\phi))}}{\sin(i) \cos(\phi)}$; $R = R_\phi (\sec^2(i) - \tan^2(i) \cos^2(\alpha))$. Here, R_ϕ is the radius in the sky plane, V_r is the line-of-sight velocity corrected for the systemic velocity, i is inclination of the disc. We adopted the inclination according to Pickering et al. (1997). The situation with the position angle is more complex since the value $PA = 296^\circ$ did not agree with our kinematics in the inner region of UGC 6614, thus we adopted $PA = 265^\circ$ for the inner 35 arcsec, and $PA = 296^\circ$ for the outer data points.

We added the ionized gas rotation curve to H I velocities from Pickering et al. (1997) and obtained the combined rotation curve

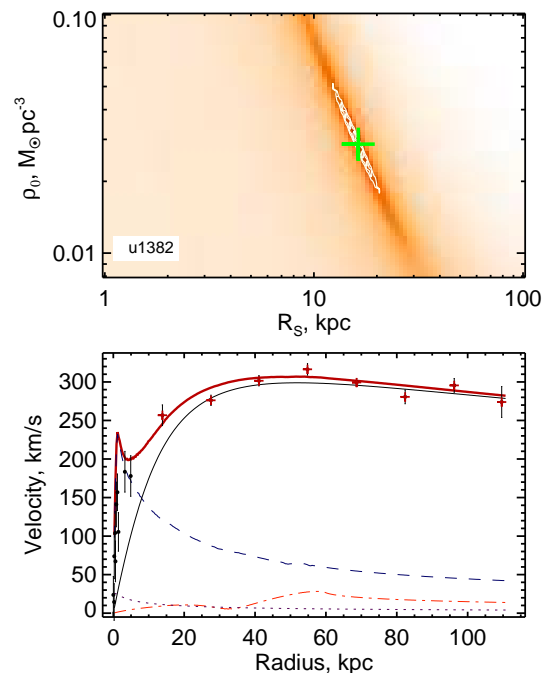


Figure 13. The results of the rotation curve decomposition for UGC 1382. The designations are the same as in Fig. 11.

for the fitting procedure. We used the structural parameters of the bulge from our analysis of the ZTF survey r -band image discussed above. We used a non-parametric definition of the disc profile as a difference between total and bulge surface brightness profiles. The r -band mass-to-light ratio of the bulge was limited in the range: 2.57. . . ,4.54. The upper value corresponds to the stellar population with the age of 12 Gyr and metallicity -0.2 for the Salpeter IMF, the lower value is for the age 12 Gyr for the Kroupa IMF. The range of disc mass-to-light ratio was estimated from the $(g - r) = 0.4$ mag colour of the disc and the M/L_r -colour relation from Roediger & Courteau (2015) taking into account the age 1 Gyr and the metallicity -0.7 dex in the region outside the dominance of bulge: 0.4. . . ,2.3. We present the fitting results for UGC 6614 in Fig. 14. As one can see from the figure, the model includes the HSB part associated with the pseudobulge component and the LSB part in a form of a non-parametrical disc. This model looks similar to that of Malin 1 and NGC 7589 constructed by Lelli et al. (2010).

de Blok et al. (2001) also performed the mass modelling for UGC 6614 using pseudo-isothermal and NFW dark halo density profiles. For the pseudo-isothermal halo, they derived the dark halo radial scale 12.18 kpc using a constant stellar R -band mass-to-light ratio 1.4. It appears to be in good agreement with the scale obtained here for the Burkert profile if one applies the transformation coefficients from Boyarsky et al. (2009). Pickering et al. (1997) obtained somewhat higher dark halo radial scale of 24.48 kpc, but they considered only H I data as the only available at the moment.

5 SCALING RELATIONS

5.1 Baryonic Tully–Fisher relation for gLSBGs

The baryonic TF (1977) relation (Sprayberry et al. 1995; McGaugh & Schombert 2015) connects the total baryonic mass (gas+stars)

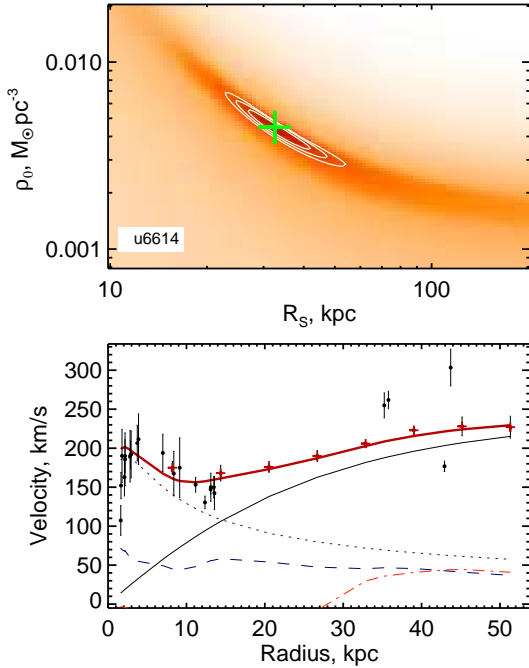


Figure 14. The results of the rotation curve decomposition for UGC 6614. The designations are the same as in Fig. 11.

to the maximal circular velocity in a galaxy. In Fig. 15, we display seven gLSBGs from our sample compared to the best-fitting linear correlations for the baryonic TF relation from the literature. Continuous thick line and open circles and dashed thick line show the relations obtained by Lelli et al. (2019) (the one with the lowest scatter) and Ponomareva et al. (2018) (the final one) correspondingly. Thin continuous and dashed lines give the uncertainties of the correlations given in the corresponding papers. Our gLSBGs are shown with the same symbols as in Fig. 9. We computed the baryonic mass as a sum of stellar disc and bulge masses from Table 6, Saburova (2018); Saburova et al. (2019), and the H I masses from Table 2. For UGC 1922, the disc mass is estimated from the photometric mass-to-light ratio. The velocities and their errors are also taken from Table 2. The errors of baryonic mass are calculated in a similar way as in Lelli et al. (2016) and include the errors of gas mass from Table 2, the uncertainty of the mass-to-light ratios of 0.11 dex following McGaugh & Schombert (2014) and the uncertainty of the luminosity of order of 10 per cent.

As one can see in Fig. 15, gLSBGs occupy the top right-hand corner of the TF relation with high rotational velocities and large baryonic masses. Most of them lie within the uncertainty of the correlation found by Lelli et al. (2019).

According to Ogle et al. (2019), the baryonic TF relation breaks for rotational velocities higher than 340 km s^{-1} , however, in our sample only UGC 1922 rotates that fast. This galaxy has the largest deviation from the relation found by Lelli et al. (2019) at the same time not being an outlier from the regression found by Ponomareva et al. (2018).

5.2 Star formation in gLSBGs

Numerous efforts were made by different teams to probe the star formation process in the low-density regime (see, e.g. Bigiel et al.

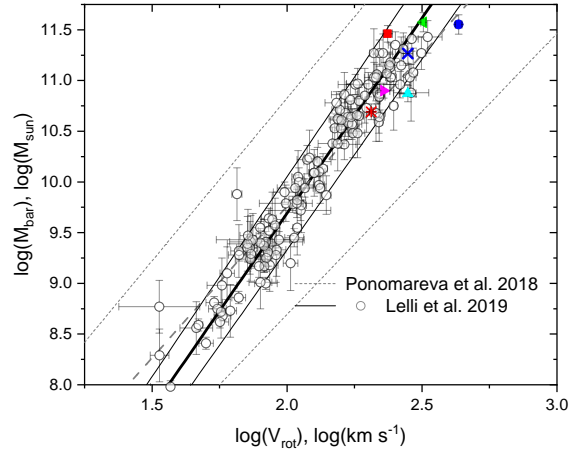


Figure 15. The position of the gLSBGs on the baryonic TF relation. Continuous and dashed lines correspond to the regressions found by Lelli et al. (2019) and Ponomareva et al. (2018). Thick lines show the relations and thin lines give the uncertainties of the parameters of the each regression. Open circles demonstrate the sample from Lelli et al. (2019). Different symbols denote different gLSBGs as in Fig. 9.

2010; Abramova & Zasov 2012; Bacchini et al. 2020) because different astrophysical phenomena might govern star formation in low- and high-density regions. The extended discs of gLSBGs represent a particularly interesting case of a low-density environment because they often have very substantial global SFRs distributed over an enormous area.

We display the integrated SFR surface densities Σ_{SFR} for the seven gLSBGs from our sample on the Schmidt–Kennicutt relation connecting Σ_{SFR} with the gas surface density in Fig. 16. For all gLSBGs except Malin 2, we plot the H I surface density instead of the total gas surface density because the reliable spatially resolved molecular gas measurements were not available for them and it is important that molecular gas density measurement are made for the same areas as the densities H I and SFR. As we also noted above the upper estimates of the molecular gas mass found for NGC 7589 and UGC 6614 are roughly 10 and 100 times lower than that of H I masses, so the inclusion of molecular gas would not change the position of the gLSBs on the Schmidt–Kennicutt diagram significantly. For Malin 2, we give the estimates integrated for the bins with available molecular gas measurement. The Σ_{SFR} value was taken from Kasparova et al. (2014) and the gas surface density from Das et al. (2010). Different symbols show the gLSBGs from our sample as indicated in the legend. For Malin 1, we took the integrated Σ_{SFR} and H I surface density from Wyder et al. (2009) and for the comparison we plot also the local value by fainter colour: Σ_{SFR} at $R = 26 \text{ kpc}$ from the centre taken from Junais et al. (2020) and the H I surface density at the same galactocentric distance from Lelli et al. (2010). For NGC 7589, UGC 1922, and UGC 6614, we calculated the Σ_{SFR} from the GALEX FUV data and plotted it against the mean H I surface density within the same radii as the UV-based SFR. The data sources for H I densities are given in Table 2. For UGC 1378, we took the estimates from Saburova et al. (2019). For UGC 1382, we estimated the average values of the SFR and H I surface densities using the data from Hagen et al. (2016), the former value was also corrected to include helium.

A thick black line shows a power law with the index of 1.41 found for spiral galaxies by de los Reyes & Kennicutt (2019) in agreement with the classical work by Kennicutt (1998). Faint open

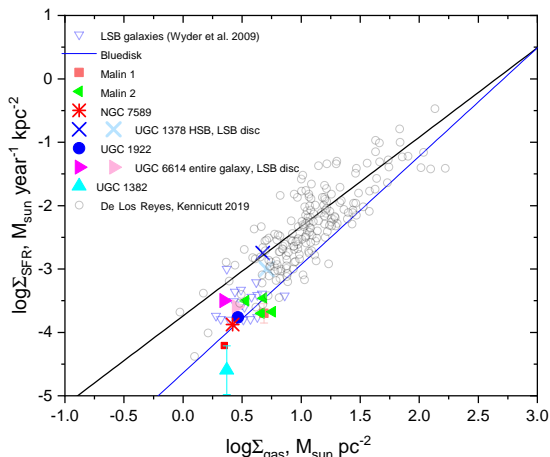


Figure 16. The SFR surface density vs gas surface density diagram. The position of each gLSBG is demonstrated by different symbols (see the legend). The black line and faint open circles correspond to the best-fitting relation by *de los Reyes & Kennicutt (2019)*. The blue line shows the best-fitting relation for the nearby galaxies with unusually high H I mass fractions from the ‘Bluedisk’ project (*Roychowdhury et al. 2015*). Faint triangles show LSB galaxies from *Wyder et al. (2009)*.

circles show the sample from *de los Reyes & Kennicutt (2019)*. Faint triangles denote LSB galaxies by *Wyder et al. (2009)*. To compare gLSBGs with extremely H I-rich galaxies we also demonstrate by a blue line the best-fitting relation for the H I surface density of the galaxies from the ‘Bluedisk’ project (*Roychowdhury et al. 2015*).

As one can see in Fig. 16, all gLSBGs besides UGC 1378 are the outliers from the *de los Reyes & Kennicutt (2019)* relation for HSB galaxies – they have too low Σ_{SFR} for the given gas surface densities. Their position is in a good agreement with the position of other low surface brightness galaxies found by *Wyder et al. (2009)*. There is an indication that the star formation efficiency might be connected to the mechanical energy of collisions of giant molecular clouds in HSB discs due to differential rotation (*Aouad et al. 2020*). However, this correlation does not hold at low gas surface densities at the same values where the local Schmidt–Kennicutt relation breaks, suggesting a different physical mechanism regulating star formation there. For example, fresh gas accretion from a filament or a gas-rich satellite will lead to the apparent decrease in the star formation efficiency. The oxygen abundance estimates for UGC 1922 disc are quite high ($12 + \log(O/H) \approx 8.6$), which argues against the accretion of metal-poor gas at least in this particular case. As it was demonstrated by *Pickering et al. (1997)* the H I surface density is below the critical density for star formation estimated using the dynamical criterion proposed by *Kennicutt (1989)* in all radii for Malin 2 and NGC 7589 and is close to the threshold value or slightly above it for UGC 6614 and Malin 1 correspondingly, it could be the reason of low values of SFR in these galaxies. At the same time *Pickering et al. (1999)* studied another giant discy galaxy with larger amount of star formation occurring within the disc and the large part of the disc possessing the gas density above the critical value, thus validating this criterion. The low efficiency of star formation could be related to significantly lower gas volume densities. As shown by *Zasov et al. (2011)*, the gas volume densities of LSB galaxies are two orders of magnitude lower than those in galaxies with normal surface brightnesses. *Abramova & Zasov (2008)* and later *Bacchini et al. (2019)*; *Yim et al. (2020)* found tight correlation between the volume densities of gas and SFR which can indicate

that taking into account the thickness of the disc could eliminate the break of the relation on the low surface densities. And indeed, as it was shown by *Bacchini et al. (2020)*, the relation for volume densities holds unbroken for a wide range of volume densities of gas and SFR including low-density regime. It could indicate that the gaseous discs of gLSBGs have the high thickness which leads to their outlying position on the gas surface density vs SFR surface density diagram. Another effect that could be important in low-density regime and could lead to the break of the gas surface density vs SFR surface density relation is the influence of the diffuse background both in SFR traces and in atomic gas which was not taken into account in the current paper (*Kumari et al. 2020*).

6 DISCUSSION

6.1 Formation scenarios of gLSBGs

The main goal of our study is to choose realistic formation scenarios of gLSBGs based on the observational data of all stellar systems of this type studied in detail up-to-date. We are trying to understand whether the processes leading to the formation of such unusual galaxies are extremely uncommon making gLSBGs ‘unique’.

Our observational data suggest that no single formation mechanism can explain all seven gLSBGs presented here. At the same time, we consider only three of the considered scenarios because each of them is consistent with all observations of at least one gLSBG: (i) a scenario involving a major merger, similar to that proposed in *Saburova et al. (2018)* and *Zhu et al. (2018)*; (ii) an explanation of unusual properties of giant LSB discs through the peculiar properties of the dark matter halo, namely the low central density and the high radial scale of the halo (*Kasparova et al. 2014*); (iii) a two-stage formation scenario in which the giant disc is formed by accretion of gas on a preexisting ‘normal’ HSB galaxy (*Saburova et al. 2019*).

In Table 7, we give a short summary of the signatures that we expect in each for the three considered scenarios. Table 8 assesses all possibilities for each galaxy in our sample.

We give the detailed discussion for the considered formation scenarios in the next subsections. But first, we explain why we do not find enough of the supporting evidence for some other mechanisms discussed in the literature.

We believe that the scenario of the outer disc formation as the result of a dwarf satellite merger (proposed by *Pefarrubia et al. (2006)* for Messier 31) has difficulties explaining the gLSB disc formation for several reasons. (i) An extended LSB disc often contains a substantial fraction of the baryonic matter in a gLSBG: their masses in UGC 1378 and UGC 1922 are 8×10^{10} and $1.8 \times 10^{10} M_{\odot}$ (*Saburova 2018*; *Saburova et al. 2019*) (see also Table 6 for the masses of the extended discs obtained in this paper). In all our cases, the masses of atomic hydrogen exceed $10^{10} M_{\odot}$ (Table 2), and it is 10–100 times more than we can expect for a dwarf galaxy satellite (see e.g. *Bettoni et al. 2003*). (ii) Another reason is that we do not observe a rapid decline in rotation curve in the peripheries of giant LSB discs (see, e.g., *Kasparova et al. 2014*) expected in the dwarf satellite merger scenario. Random orientation and high eccentricity of the orbits of infalling satellites predicted by some numerical simulations in the Lambda cold dark matter (Λ CDM) cosmology will likely lead to the loss of angular momentum by both gas and stars and form a dynamically hot stellar halo with the gas sinking to the centre rather than forming a disc. A potential solution exists if numerous satellites infall onto the gLSBG progenitor from a thin vast rotating plane like the ones discovered around

Table 7. Expected signatures of the proposed formation scenarios of gLSBGs.

Signatures \ scenario	Major merger	Sparse dark halo	Gas accretion on a preformed galaxy
DM parameters agree with the giant disc radius	No	Yes	No
Two discs with different scale lengths	No	No	Yes
Dynamical overheating of the disc	Expected	Not expected	Not expected
Disturbed morphology	Expected	Not expected	Not expected
Presence of satellites	Expected	Not expected	Not expected

Table 8. Assessment on the proposed formation scenarios for each galaxy in our sample.

	Major merger	Sparse Dark halo	Gas accretion on a preformed galaxy
Malin 1	Possibly	Uncertain	Possibly
Malin 2	No	Yes	No
NGC 7589	No	Yes	Yes
UGC 1378	No	No	Yes
UGC 1382	Possibly	No	Possibly
UGC 1922	Yes	Possibly	No
UGC 6614	No	Yes	Possibly

the Andromeda galaxy (Ibata et al. 2013) and Centaurus A (Müller et al. 2018) suspected to be aligned with the large-scale structure of the Universe (Libeskind et al. 2015). Such planes despite being recognized as one of the ‘small scale problems’ of Λ CDM (Bullock & Boylan-Kolchin 2017), are successfully reproduced in numerical simulations (see e.g. Ibata et al. 2014; Santos-Santos et al. 2020). However, the feasibility of this gLSBG formation scenario still remains in question because most known gLSBGs do not have many satellites observed in their vicinity, while some such satellites would inevitably survive if a massive accretion of a satellite ring/plane occurred in the recent past or is currently happening.

Another scenario explaining the formation of the expanding ring-like giant LSB structure by a bygone head-on collision with a massive intruder proposed by Mapelli et al. (2008) also seems to be unlikely, since none of the expected signatures of this model are found in the deep images and colour profiles of gLSBGs (Kasparova et al. 2014; Boissier et al. 2016; Hagen et al. 2016). In addition, the progenitor in this model should already be a massive LSB-galaxy which makes it even less realistic and does not really explain the formation of a giant LSB disc.

6.1.1 The origin of the central regions of gLSBGs

One possible way to understand the evolution of a galaxy is to explore its inner regions and a nucleus. The structure of the bulge and the mass of the central black hole can help us to better understand the merger history of the galaxy because they are expected to co-evolve (see e.g. Kormendy & Ho 2013, and references therein).

One can notice from Table 2 that gLSBGs host AGN in six out of seven considered cases⁹ – such AGN occurrence rate is extremely high compared to HSB galaxies (Ho et al. 1997). The high frequency of low-luminosity AGN signatures in gLSBGs compared to other late-type galaxies was also noticed by Schombert (1998).

Another detail that becomes evident when looking at Fig. 17

⁹ The seventh galaxy – UGC 1378 may also contain an AGN according to Schombert (1998).

and Table 2 is that gLSBGs tend to have low masses of central black holes (M_{BH}) which sometimes even get close to the intermediate-mass black hole regime. Subramanian et al. (2016) noted a systematic offset of LSB galaxies from the $M_{BH} - \sigma_*$ relation where stellar velocity dispersion σ_* is averaged within one effective radius. According to Subramanian et al. (2016), LSB galaxies tend to have lower masses of black holes than what is expected for the values of velocity dispersions in their bulges.

In Fig. 17, we show the $M_{BH} - \sigma_*$ for gLSBGs from our sample and compare them to a large sample of ‘normal’ galaxies and the regression found by Sahu et al. (2019). The stellar velocity dispersion measurements of gLSBGs come from this study and from Reshetnikov et al. (2010); Saburova (2018); Saburova et al. (2019). The adopted black hole masses and corresponding data sources are given in Table 2. Open and filled circles demonstrate early- and late-type galaxies from Sahu et al. (2019). We use the regression obtained by Sahu et al. (2019) for both early- and late-type galaxies (the situation does not change significantly if we consider the regression found only for galaxies with discs). From Fig. 17 it is clear that three of the five gLSBGs with measured black hole masses deviate from the relation found by Sahu et al. (2019), and UGC 6614 lies on the margin of the 1σ range having a slightly lower M_{BH} than expected for its σ_* . This can indicate that the bulges of the considered gLSBGs did not co-evolve with the central black holes and either were formed *in situ* via secular evolution or grew via minor mergers, which are not expected to increase the M_{BH} mass because dwarf galaxies do not often host central massive black holes. Kormendy et al. (2011), who reported the pseudobulge classification for galaxies with dynamically detected black holes, found out that the black hole masses correlate very little at best with pseudobulge properties.

Graham (2014) showed that pseudobulges are difficult to identify and their classification is quite subjective. However, it should be noted that Malin 1, Malin 2 (for a model with two discs), UGC 6614, UGC 1378, and UGC 1922 have Sérsic indices $n < 2$ and their bulges do not look rounder than the discs which could be the main argument for their classification as pseudobulges. It makes the high frequency of AGN activity among gLSBGs even more interesting, since the AGN signatures in the emission line ratios decreases significantly for the galaxies with pseudobulges (Yesuf et al. 2020). It could indicate the presence of the current gas supply to the centres of gLSBGs leading to the AGN activity and related to the accretion of material either from a filament or from a gas-rich satellite. The counterrotation of gas that we observe in UGC 1382 and UGC 1922 could also be related to the external gas accretion. Khoperskov et al. (2020) showed that the AGN is efficiently triggered by the retrograde gas infall into a galaxy.

At the same time, according to Kormendy et al. (2011), the growth of central black holes in pseudobulges is driven rather *not* by global processes like major merger but more by local and stochastic processes. In this regime, black holes are not expected to co-evolve

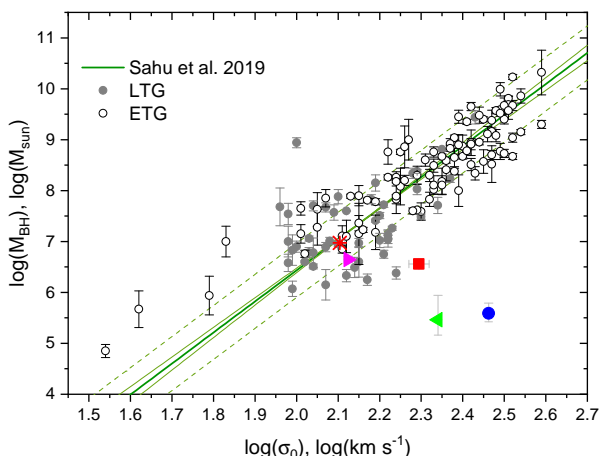


Figure 17. The gLSB galaxies with available measurements of central black hole masses on the mass of the black hole versus central velocity dispersion ($M_{BH} - \sigma_*$) diagram. Open and filled circles show early- and late-type galaxies from Sahu et al. (2019). Continuous thick line shows the best-fitting relation found by Sahu et al. (2019) for the combined sample of early- and late-type galaxies. Thin lines show the 1σ uncertainty of the slope and the intercept of the relation. Dashed lines represent the $\pm 1\sigma$ scatter in their data. Different symbols depict different gLSBGs in the same manner as in Fig. 9. The clear outliers are Malin 1, Malin 2, and UGC 1922.

with the bulges and hence their masses might not correlate with the properties of bulges – exactly what we see in Fig. 17 for gLSBGs except NGC 7589 (and possibly UGC 6614). This could imply that there were not a lot of major merger events in the history of most gLSBGs and their baryonic masses were accumulated by some other processes. The study of globular clusters in UGC 6614 using deep HST images also provides evidence that the galaxy accumulated its stellar mass through sporadic star formation activity and its star formation history lacks dominant starburst events which could be induced by major mergers Kim (2011).

Taking into account all these facts, we conclude the observed properties of central parts and central black holes of gLSBGs support the scenario of the gLSB disc formation by external cold gas accretion either from cosmic filaments or from gas-rich satellites and disfavour their formation by major mergers.

6.1.2 Gas accretion on a preexisting galaxy (HSB+LSB)

About a decade ago (Lelli et al. 2010) it became clear that some gLSBGs have a complex structure consisting of an inner ‘normal’ HSB early-type spiral galaxy immersed in an extended LSB disc. Discs of such HSB+LSB galaxies cannot be described by a single exponential profile. We expect that the extent of the dark halo in such galaxies is in good agreement with the R_{25} size of the HSB part. The relatively low radial scale of the dark matter halo can indicate that the accreted gas could have the angular momentum differing from that of the HSB disc. In this case, there is a two-stage build-up of the galactic disc and the main question is: where did the additional material (gas and stars?) for the LSB disc formation come from? The environment of such galaxies has to, first, have a source for cold gas accretion, and secondly, a possible close interaction should not tear off the LSB periphery of the disc by tidal effects. If the additional material originates from a cosmic filament, then the environment of such a galaxy should be sparse. Observational data for four of seven gLSBGs do not contradict this scenario.

In the case of Malin 1 several facts speak in favour of this formation mechanism. Malin 1 shows a complex double disc structure including HSB and LSB parts (Lelli et al. 2010). The outer part is much bluer than the inner one (Galaz et al. 2015). The age of the extended disc is young (Boissier et al. 2016). The current burst of star formation in the extended disc could have been induced by a recent minor merger about 1 Gyr ago (Reshetnikov et al. 2010).

NGC 7589 also demonstrates the HSB+LSB structure (Lelli et al. 2010). The positional angle of the major axis of NGC 7589 changes with radius evident from both, photometric analysis and the twist of isoveLOCITY lines in the H α velocity field published by Pickering et al. (1997). This can indicate the external origin of the outer LSB structure. This galaxy also possesses a massive companion with the velocity difference of roughly 100 km s^{-1} (NGC 7603 which has disturbed spiral arms and is twice the size of NGC 7589). Both, the extended blue disc of NGC 7589 and the disturbed appearance of NGC 7603 could be the traces of past interactions of these two galaxies. The elongated thin spiral arms could be possibly short-living and related to the density wave in the disc induced by a recent tidal interaction between these two systems. In this case, the interaction ‘lit up’ the giant disc of NGC 7589 which became more visible with the spiral arms and the blue colour of the extended disc because an interaction induced burst of star formation.

UGC 1378 was studied in details in Saburova et al. (2019) who proposed a two-step formation scenario in which the gas accretion onto a ‘typical’ HSB spiral galaxy similar to the Milky Way led to the formation of the extended LSB disc.

UGC 1382 is a lenticular galaxy with an extended LSB disc. Our data reveal that the ionized gas in the centre rotates in the opposite sense to the old stellar disc, but it co-rotates with the giant H α disc described by Hagen et al. (2016). That is, there is a counterrotation of the large-scale discs along all distances from the galaxy center. Assuming a natural evolutionary link between the extended H α disc and the LSB disc we expect that the stellar LSB disc also counterrotates with respect to the HSB part. Our absorption-line spectra unfortunately do not reach the LSB part and cannot be used to support or refute this hypothesis. However, a counterrotating LSB disc might contribute to the stellar LOSVD even in the HSB part of the galaxy. This hypothesis is supported by non-zero values of $h3$ and $h4$ profiles (see right-hand panel Fig. 5) suggestive of a non-Gaussian shape of the stellar LOSVD. To check this idea we recovered stellar LOSVD in a non-parametric shape applying methodology from Katkov et al. (2011, 2016). Unfortunately, we did not find clear signs of the stellar counterrotation like two distinct peaks or long tails in the LOSVD. We detected a slightly non-Gaussian shape and a peaked structure of the LOSVD slightly varying from one bin to another likely caused by the noise in the data. This means that the LSB stellar disc is too faint to be detected in the region dominated by the HSB disc. Therefore, only dedicated ultradeep spectroscopy of the external LSB disc might confirm our expectation about counterrotation of the stellar LSB part in this galaxy.

The H α disc of UGC 1382 with a rotational velocity of 280 km s^{-1} (Hagen et al. 2016) has signs of ongoing star formation (as we can see by the presence of UV-bright spirals in GALEX images). Our spectrum fitting gives very old age of the central part with the trend of the age decreasing with the radius, i.e. a negative age gradient (see Fig. 5). According to Hagen et al. (2016) the age of the LSB spirals is 4 Gyr older than the HSB part. Such a difference with our data can be associated with the age estimation methodology (spectral vs. photometric) and the adopted star formation histories (SSP vs. exponentially declining). We believe that

the counterrotation of the large-scale H α disc could indicate the gas accretion from a filament (Algorry et al. 2014) on a preexisting early-type disc galaxy (probably, S0).

6.1.3 Sparse dark halo

The second scenario is a non-catastrophic formation of a single disc with a large radial scale in a sparse dark matter halo (large radial scale and low central density). In four cases, Malin 2, NGC 7589, UGC 6614 and UGC 1922, the radial scale of the dark halo is in agreement with the size of an extended disc. One should keep in mind the uncertainties of dark matter halo parameters for UGC 1922 and NGC 7589 are too high to make firm statements on the shallowness of their halo. Normal-sized LSB galaxies are probably formed in haloes with low concentrations of a rapidly rotating host as a result of the centrifugal equilibrium (Mo et al. 1998; Bullock et al. 2001; Kim & Lee 2013), and the extreme cases of such haloes can host gLSBGs. The reasons for the formation of a dark halo with such properties can be found in numerical models of protohalo mergers and they can probably be related to the low-density environment (Macciò et al. 2007).

6.1.4 Major merger

In the modern galaxy formation framework, massive galaxies with stellar mass $\sim 10^{11} M_{\odot}$ should have experienced at least one major merger in their lifetime (Rodríguez-Gomez et al. 2015). However, such events are more likely to occur in a dense environment. It is expected that a galaxy formed in this way will have a hot stellar disc (if the disc survives at all) and, probably, perturbed morphology (Saburova et al. 2018). However, all existing data for gLSBGs except UGC 1922, show the contrary. The prominent well-organized spiral structure can indirectly evidence that the discs of most known gLSBGs are thin and, consequently, are not significantly overheated (Zasov et al. in preparation). To confirm the catastrophic scenario, we need to estimate the stellar velocity dispersion in the region of the LSB disc of a gLSBGs. This is a very challenging observational task. The modern spectrographs allow astronomers to probe velocity dispersions down to 10–15 km s $^{-1}$ at surface brightnesses as low as $\mu_g = 25.5$ mag arcsec $^{-2}$ in UDGs (Chilingarian et al. 2019), which should, in principle, be sufficient for some gLSB discs. However, because of young and potentially metal-poor stellar populations anticipated in gLSBGs, their spectra are expected to have much shallower absorption lines leading to the drastic increase of uncertainties of internal kinematics for the spectra of the same depth (Chilingarian & Grishin 2020). A viable solution is to find edge-on gLSBGs where the surface brightness is boosted because of the line-of-sight integration through the disc.

Zhu et al. (2018) proposed a major merging scenario for Malin 1 which does not contradict to its observed properties including the absence of the gradient of the stellar age in the disc. We also observe two red satellites projected on-to the LSB disc of Malin 1 (Reshetnikov et al. 2010; Galaz et al. 2015) which could be the survived remnants of larger galaxies that interacted with it. Their structural properties put them into the rare class of compact elliptical galaxies (Chilingarian et al. 2009a) proven to be formed via tidal stripping of massive progenitors (Chilingarian & Zolotukhin 2015). A low-luminosity compact galaxy is also orbiting UGC 1382. One should keep in mind, however, that the study by Zhu et al. (2018) does not mention whether they succeeded to reproduce the light profile described by a sum of two exponential components, as it was demonstrated for Malin 1 by Lelli et al. (2010).

In the case of Malin 2 we can exclude the major merger scenario since its disc is only mildly dynamically overheated and Kasparova et al. (2014) observed a steep metallicity gradient for the gas in the disc which is likely to be flattened during mergers (see, e.g. Zasov et al. 2015, and references therein).

UGC 1922 described in detail in Saburova et al. (2018) seems to differ from all other other known gLSBGs. It has a strongly overheated stellar disc with clumpy irregular spiral arms. The ionized gas in the inner region counterrotates with respect to the outer part of the galaxy. Saburova et al. (2018) reproduced most of the observed features of the galaxy in the model of an in-plane merger of giant Sa and Sd galaxies. Therefore, UGC 1922 is likely a result of a major merger. This assumption is also supported by the fact that this is the only galaxy in our sample deviating from the TF relation.

6.2 Comparison with other galaxies with extended LSB and XUV discs

The demarcation between gLSBGs and ‘normal’ extended LSB galaxies in the parameter space is rather arbitrary. We limit this study to the objects disc radii larger than 50 kpc, which we consider as an informal boundary for gLSBGs. At the same time, LSB galaxies with moderate sizes have similar properties to gLSBGs and might have similar formation scenarios. Therefore, it might be useful to compare our sample against extended LSBGs with disc scale lengths somewhat smaller than 50 kpc. One prominent case is NGC 5533 with the LSB disc with the scale length of approximately 9 kpc (Noordermeer & van der Hulst 2007). Despite being substantially smaller than UGC 1378, this galaxy has a similar complex structure that contains an ‘HSB galaxy’ embedded in extended LSB disc (Sil’chenko et al. 1998). Since the two galaxies have similar structural properties even though at different spatial scales, it will be helpful to compare their general characteristics. Stellar populations in the HSB part of NGC 5533 are also similar to those of UGC 1378. The HSB stellar disc of NGC 5533 is metal-poor and has an intermediate age (2 – 4 Gyr). The bulge has solar stellar metallicity and a slightly older age of 6 – 7 Gyr (I. Katkov, private communication). The H α rotation curve of NGC 5533 is declining (Noordermeer et al. 2007), which results in a small radial scale of the dark halo (Noordermeer 2006). The complex HSB+LSB structure and a short radial scale of the dark halo suggests that the extended LSB disc of NGC 5533 (similarly to UGC 1378) could have been formed by the accretion of gas onto a preexisting early-type spiral.

Another extended LSB system is NGC 5383 with the disc scale length of 9.7 kpc (van der Kruit & Bosma 1978). This galaxy has a strong bar and extended LSB spiral structure similar to that of NGC 7589. The system also has a companion UGC 8877 at the distance of roughly 30 kpc with the velocity difference of 100 km s $^{-1}$. We see the bifurcation of the spiral arms of NGC 5383. Tidal forces could impose a new mode of the density wave in the disc, which gave the rise to the faint spiral arms like, for example, in the interacting system Arp 82 (Zasov et al. 2019).

Systems morphologically similar to UGC 1382, but with smaller discs can be found in the deep images from the MATLAS project (Mass Assembly of early-Type GaLaxies with their fine Structures Duc et al. 2015). One example is UGC 9519, a dwarf S0 galaxy surrounded by an extended LSB spiral disc with a radius of ~ 30 kpc. Sil’chenko et al. (2019) found out that gas in the inner part of UGC 9519 rotates in a nearly polar plane with respect to the stellar disc and the outer disc is decoupled from the main body of the galaxy. This could indicate that gas was accreted from external sources (Sil’chenko et al. 2019).

Starforming gLSBGs can be considered as an extension of the class of galaxies with extended ultraviolet discs (XUV discs [Gil de Paz et al. 2005](#); [Thilker et al. 2005, 2007](#)) to larger disc sizes and thus could have evolved in a similar way. [Hagen et al. \(2016\)](#) classified UGC 1382 as a Type I XUV disc similar to the prototypical XUV disc galaxies M 83 and NGC 4625 ([Gil de Paz et al. 2005](#); [Thilker et al. 2005](#)). [Boissier et al. \(2016\)](#) also notes that Malin 1 could be an extreme case of an antitruncated XUV disc. According to [Thilker et al. \(2007\)](#), Type I XUV discs are found in upto 20 per cent of galaxies and span the entire range of Hubble types. The global characteristics of galaxies with XUV discs are similar to those of ‘normal’ galaxies, which can indicate that the formation of an XUV disc could be a stage of ‘normal’ galaxy formation process. [Thilker et al. \(2007\)](#) pointed out that an interaction could trigger the formation of an XUV disc, or, in other words, trigger a burst of star formation in the extended gaseous disc which would have remained passive and ‘dark’ otherwise. Another possible trigger may be a high specific rate of gas accretion (i.e. per unit stellar mass).

It is interesting to compare gLSBGs with the famous Hoag’s Object, an unusual giant ring galaxy in a low-density environment discovered by [Hoag \(1950\)](#). The blue and young ring surrounds an elliptical galaxy hosting old metal-rich stellar population ([Finkelman et al. 2011](#)). The radius of the ring is about 25 kpc and it has a clearly visible spiral-like pattern. [Finkelman et al. \(2011\)](#) proposed that the peculiar structure and observed properties of the Hoag’s Object are the result of the gas accretion onto a preexisting elliptical galaxy. The Hoag’s Object could thus be a special case of a “failed” gLSBGs in which instead of a giant LSB disc, the star-forming ring was formed due to some specific properties of the system, e.g. a triaxial potential of the elliptical galaxy, which could lead to the prominent gap between the core and the ring.

There exist LSB-systems with complex HSB+LSB structures like that in many gLSBGs but with more moderate sizes. Interesting example of such system is Ark 18 residing in the Eridanus void with an extended blue LSB disc and a bright central elliptically-shaped part which is probably the result of a dwarf-dwarf merger ([Egorova et al. 2021](#)).

6.3 Comparison of gLSBGs with oversized HSB galaxies

[Ogle et al. \(2016\)](#) found out that about 6 per cent of the most optically luminous galaxies have giant HSB discs with isophotal diameters of 55 – 140 kpc. This sample was extended by [Ogle et al. \(2019\)](#) which also included non-star-forming ‘super-lenticulars’ in addition to superspirals and giant elliptical galaxies. A small fraction of the superluminous galaxies had disturbed morphology indicating recent mergers. Similarly to gLSBGs, super disc galaxies are red inside and blue outside which could be consistent with the on-going growth of the disc by accretion and minor mergers ([Ogle et al. 2019](#)). [Kasparova et al. \(2020\)](#) studied in detail the edge-on ‘super-lenticular’ NGC 7572 with an excessively massive thick disc and concluded that the thin disc growth was likely stopped prematurely by the dense cluster environment. Otherwise, this object would have become an enormous ‘superspiral’ if it could continue to grow its disc from an external gas supply.

[Saburova \(2018\)](#) also studied giant HSB disc galaxies at lower redshifts compared to those from the sample of [Ogle et al. \(2016\)](#) and using different selection criterion, the isophotal radius rather than luminosity used in [Ogle et al. \(2016\)](#). [Saburova \(2018\)](#) derived the parameters of dark haloes of giant HSB galaxies and concluded that they tend to have high halo masses and radial scales in agreement with their large disc radii. Thus, [Saburova \(2018\)](#) proposed that the

size of HSB giants is due to the sparse dark halo being similar to the formation scenario by [Kasparova et al. \(2014\)](#) proposed for the gLSBG Malin 2.

An interesting case is the giant spiral galaxy LEDA 1970716 discovered by visual inspection of DECaLS optical images. It has an asymmetric spiral arm with blue clumps of star formation which extends out to 120 kpc from the centre, whose formation could have been induced by the interaction with neighbouring galaxies. This example demonstrates the possibility of the giant LSB disc formation by gravitational interactions (flybys).

7 SUMMARY

We collected long-slit spectral observations for four gLSBGs galaxies in addition to the three systems with the data available in the literature. We also performed surface photometric analysis for NGC 7589 and UGC 6614 on deep archival images. We analysed all available information for the sample of seven gLSBGs and compared them to galaxies of moderate sizes and to giant HSB galaxies (‘superspirals’).

Observational data favor the external origin of the giant LSB discs for most gLSBGs. For NGC 7589, UGC 1378, and UGC 1382, we argue for the two-stage formation scenario in which the extended LSB disc is a result of gas accretion on a preexisting early-type galaxy. There also exist gLSBGs like UGC 1922 which were likely formed by a major merger. For Malin 1 and UGC 1382, we also can not exclude the major merger hypothesis. Some alternative formation scenarios are also feasible. For Malin 2, UGC 6614 and possibly NGC 7589, we found high radial scale and low central density of their dark haloes, so the unusual properties of their discs could be dictated by the sparse dark matter haloes.

The proposed formation scenarios are supported by the following observed properties of gLSBGs:

- We detected a counterrotation of ionized gas in the inner parts of two out of seven considered gLSBGs. Similar high statistical frequency of the kinematically decoupled kinematics is observed in isolated lenticular galaxies ([Katkov et al. 2014](#)), where the external origin of gas via accretion is a preferred scenario.
- The SFR surface densities of gLSBGs are too low for their gas content, which can be a result of the inefficient star formation, e.g. because of the low gas volume density or very recent accretion of gas.
- At least six out of seven presented gLSBGs host active galactic nuclei. Such high AGN rate requires the presence of gas supply reaching the central regions of the galaxies. At the same time, the central black hole masses appear to be significantly lower than expected for the obtained central stellar velocity dispersions, in agreement with previous findings by [Ramya et al. \(2011\)](#); [Subramanian et al. \(2016\)](#). This can indicate that there were not many major merger events in the history of gLSBGs similar to galaxies with smaller bulges hosting active intermediate-mass black holes ([Chilingarian et al. 2018](#)).
- We performed the mass modelling of optical + H α rotation curves of the seven gLSBGs using the Burkert dark matter density profile. The derived parameters of dark haloes show different behavior compared to the LSB disc radius and R_{opt} which can indicate different formation scenarios of the considered galaxies.
- Stellar populations in the central parts of most of the presented gLSBGs are old and metal-rich arguing for a two-stage gLSBG formation.

We conclude that the seven presented gLGBGs do not form a homogeneous class of objects and one should consider several alternatives for their formation scenarios, most of which require an external origin of material to form gLSB discs.

DATA AVAILABILITY

The data underlying this paper will be shared upon request to the corresponding author.

ACKNOWLEDGEMENTS

We thank the anonymous referee for the valuable and encouraging comments. We are grateful to Anatoly Zasov, Françoise Combes, and Frédéric Bournaud for fruitful discussion. The spectral data reduction and interpretation of the results were supported by the Russian Science Foundation (RScF) grant No. 19-12-00281. The mass modelling of the rotation curves was done with the support of the Russian Science Foundation (RScF) grant No. 19-72-20089. IC's research is supported by the Telescope Data Center of the Smithsonian Astrophysical Observatory. We acknowledge the usage of the HyperLeda database (<http://leda.univ-lyon1.fr>). This research has been supported by the Interdisciplinary Scientific and Educational School of Moscow University "Fundamental and Applied Space Research". KG acknowledges the support from the Foundation of development of theoretical physics and mathematics 'Basis' (category: students). Observations conducted with the 6-m telescope of the Special Astrophysical Observatory of the Russian Academy of Sciences carried out with the financial support of the Ministry of Science and Higher Education of the Russian Federation (including agreement No. 05.619.21.0016, project ID RFMEFI61919X0016). Based on observations obtained with MegaPrime/MegaCam, a joint project of CFHT and CEA/DAPNIA, at the Canada-France-Hawaii Telescope (CFHT) which is operated by the National Research Council (NRC) of Canada, the Institut National des Science de l'Univers of the Centre National de la Recherche Scientifique (CNRS) of France, and the University of Hawaii. This study is based in part on data collected at Subaru Telescope and retrieved from the Hyper-SuprimeCam data archive system, which is operated by Subaru Telescope and Astronomy Data Center at National Astronomical Observatory of Japan and on observations obtained at the international Gemini Observatory (proposals GN-2005B-Q-61 and GN-2006B-Q-41, data retrieved from the Gemini Science Archive, <http://archive.gemini.edu/>), a program of NSF's NOIRLab, which is managed by the Association of Universities for Research in Astronomy (AURA) under a cooperative agreement with the National Science Foundation on behalf of the Gemini Observatory partnership: the National Science Foundation (United States), National Research Council (Canada), Agencia Nacional de Investigación y Desarrollo (Chile), Ministerio de Ciencia, Tecnología e Innovación (Argentina), Ministério da Ciência, Tecnologia, Inovações e Comunicações (Brazil), and Korea Astronomy and Space Science Institute (Republic of Korea). The Legacy Surveys consist of three individual and complementary projects: the Dark Energy Camera Legacy Survey (DECaLS; NOAO Proposal ID 2014B-0404; PIs: David Schlegel and Arjun Dey), the Beijing-Arizona Sky Survey (BASS; NOAO Proposal ID 2015A-0801; PIs: Zhou Xu and Xiaohui Fan), and the Mayall z-band Legacy Survey (MzLS; NOAO Proposal ID 2016A-0453; PI: Arjun Dey).

REFERENCES

Abramova O. V., Zasov A. V., 2008, *Astronomy Reports*, **52**, 257

- Abramova O. V., Zasov A. V., 2012, *Astronomy Letters*, **38**, 755
 Afanasiev V. L., Moiseev A. V., 2005, *Astronomy Letters*, **31**, 194
 Aihara H., et al., 2019, *PASJ*, **71**, 114
 Algorry D. G., Navarro J. F., Abadi M. G., Sales L. V., Steinmetz M., Piontek F., 2014, *MNRAS*, **437**, 3596
 Aouad C. J., James P. A., Chilingarian I. V., 2020, *MNRAS*, **496**, 5211
 Bacchini C., Fraternali F., Iorio G., Pezzulli G., 2019, *A&A*, **622**, A64
 Bacchini C., Fraternali F., Pezzulli G., Marasco A., 2020, *A&A*, **644**, A125
 Barth A. J., 2007, *AJ*, **133**, 1085
 Bell E. F., McIntosh D. H., Katz N., Weinberg M. D., 2003, *ApJS*, **149**, 289
 Bellm E. C., et al., 2019, *PASP*, **131**, 018002
 Bertin E., 2010, SWarp: Resampling and Co-adding FITS Images Together (ascl:1010.068)
 Bettoni D., Galletta G., Garcia-Burillo S., 2003, *A&A*, **405**, 5
 Bigiel F., Leroy A., Walter F., Blitz L., Brinks E., de Blok W. J. G., Madore B., 2010, *AJ*, **140**, 1194
 Boissier S., et al., 2008, *ApJ*, **681**, 244
 Boissier S., et al., 2016, *A&A*, **593**, A126
 Bothun G. D., Impey C. D., Malin D. F., Mould J. R., 1987, *AJ*, **94**, 23
 Bothun G. D., Schombert J. M., Impey C. D., Schneider S. E., 1990, *ApJ*, **360**, 427
 Boyarsky A., Ruchayskiy O., Iakubovskiy D., Maccio' A. V., Malyshev D., 2009, arXiv e-prints, p. arXiv:0911.1774
 Brodie J. P., Romanowsky A. J., Strader J., Forbes D. A., 2011, *AJ*, **142**, 199
 Bullock J. S., Boylan-Kolchin M., 2017, *ARA&A*, **55**, 343
 Bullock J. S., Kolatt T. S., Sigad Y., Somerville R. S., Kravtsov A. V., Klypin A. A., Primack J. R., Dekel A., 2001, *MNRAS*, **321**, 559
 Burkert A., 1995, *ApJ*, **447**, L25
 Cao T.-W., et al., 2017, *AJ*, **154**, 116
 Cappellari M., Emsellem E., 2004, *PASP*, **116**, 138
 Chilingarian I. V., Grishin K. A., 2020, *PASP*, **132**, 064503
 Chilingarian I., Zolotukhin I., 2015, *Science*, **348**, 418
 Chilingarian I., Prugniel P., Sil'chenko O., Koleva M., 2007a, in Vazdekis A., Peletier R., eds, IAU Symposium Vol. 241, IAU Symposium. pp 175–176 (arXiv:0709.3047), doi:10.1017/S1743921307007752
 Chilingarian I. V., Prugniel P., Sil'chenko O. K., Afanasiev V. L., 2007b, *MNRAS*, **376**, 1033
 Chilingarian I., Cayatte V., Revaz Y., Dodonov S., Durand D., Durret F., Micol A., Slezak E., 2009a, *Science*, **326**, 1379
 Chilingarian I. V., Novikova A. P., Cayatte V., Combes F., Di Matteo P., Zasov A. V., 2009b, *A&A*, **504**, 389
 Chilingarian I. V., Zolotukhin I. Y., Katkov I. Y., Melchior A.-L., Rubtsov E. V., Grishin K. A., 2017, *ApJS*, **228**, 14
 Chilingarian I. V., Katkov I. Y., Zolotukhin I. Y., Grishin K. A., Beletsky Y., Boutsia K., Osip D. J., 2018, *ApJ*, **863**, 1
 Chilingarian I. V., Afanasiev A. V., Grishin K. A., Fabricant D., Moran S., 2019, *ApJ*, **884**, 79
 Das M., O'Neil K., Vogel S. N., McGaugh S., 2006, *ApJ*, **651**, 853
 Das M., Boone F., Viallefond F., 2010, *A&A*, **523**, A63
 Dey A., et al., 2019, *AJ*, **157**, 168
 Di Paolo C., Salucci P., Erskurt A., 2019, *MNRAS*, **490**, 5451
 Duc P.-A., et al., 2015, *MNRAS*, **446**, 120
 Egorova E. S., Egorov O. V., Moiseev A. V., Saburova A. S., Grishin K. A., Chilingarian I. V., 2021, arXiv e-prints, p. arXiv:2103.00211
 Fall S. M., Efstathiou G., 1980, *MNRAS*, **193**, 189
 Finkelman I., Moiseev A., Brosch N., Katkov I., 2011, *MNRAS*, **418**, 1834
 Francis K. J., Drinkwater M. J., Chilingarian I. V., Bolt A. M., Firth P., 2012, *MNRAS*, **425**, 325
 Freeman K. C., 1970, *ApJ*, **160**, 811
 Galaz G., Herrera-Camus R., Garcia-Lambas D., Padilla N., 2011, *ApJ*, **728**, 74
 Galaz G., Milovic C., Suc V., Busta L., Lizana G., Infante L., Royo S., 2015, *ApJ*, **815**, L29
 Gil de Paz A., et al., 2005, *ApJ*, **627**, L29
 Graham A. W., 2014, in Seigar M. S., Treuhardt P., eds, Astronomical Society of the Pacific Conference Series Vol. 480, Structure and Dynamics of Disk Galaxies. p. 185 (arXiv:1311.7207)
 Greco J. P., et al., 2018, *ApJ*, **857**, 104

- Hagen L. M. Z., et al., 2016, *ApJ*, **826**, 210
- Ho L. C., Filippenko A. V., Sargent W. L. W., 1997, *ApJ*, **487**, 568
- Hoag A. A., 1950, *AJ*, **55**, 170
- Huchra J. P., et al., 2012, *ApJS*, **199**, 26
- Ibata R. A., et al., 2013, *Nature*, **493**, 62
- Ibata R. A., Ibata N. G., Lewis G. F., Martin N. F., Conn A., Elahi P., Arias V., Fernandez N., 2014, *ApJ*, **784**, L6
- Jackson R. A., Martin G., Kaviraj S., Laigle C., Devriendt J., Dubois Y., Pichon C., 2020, arXiv e-prints, p. [arXiv:2004.00023](https://arxiv.org/abs/2004.00023)
- Jester S., et al., 2005, *AJ*, **130**, 873
- Junais Boissier S., 2019, in Di Matteo P., Creevey O., Crida A., Kordopatis G., Malzac J., Marquette J. B., N'Diaye M., Venot O., eds, SF2A-2019: Proceedings of the Annual meeting of the French Society of Astronomy and Astrophysics. p. Di
- Junais et al., 2020, arXiv e-prints, p. [arXiv:2003.09492](https://arxiv.org/abs/2003.09492)
- Kasparova A. V., Saburova A. S., Katkov I. Y., Chilingarian I. V., Bizyaev D. V., 2014, *MNRAS*, **437**, 3072
- Kasparova A. V., Katkov I. Y., Chilingarian I. V., 2020, *MNRAS*, **493**, 5464
- Katkov I. Y., Chilingarian I. V., 2011, in Evans I. N., Accomazzi A., Mink D. J., Rots A. H., eds, Astronomical Society of the Pacific Conference Series Vol. 442, Astronomical Data Analysis Software and Systems XX. p. 143 ([arXiv:1012.4125](https://arxiv.org/abs/1012.4125))
- Katkov I., Chilingarian I., Sil'chenko O., Zasov A., Afanasiev V., 2011, *Baltic Astronomy*, **20**, 453
- Katkov I. Y., Sil'chenko O. K., Afanasiev V. L., 2014, *MNRAS*, **438**, 2798
- Katkov I. Y., Sil'chenko O. K., Chilingarian I. V., Uklein R. I., Egorov O. V., 2016, *MNRAS*, **461**, 2068
- Kennicutt Robert C. J., 1989, *ApJ*, **344**, 685
- Kennicutt Robert C. J., 1998, *ARA&A*, **36**, 189
- Khoperskov S., et al., 2020, arXiv e-prints, p. [arXiv:2010.11581](https://arxiv.org/abs/2010.11581)
- Kim J. H., 2011, *Journal of Korean Astronomical Society*, **44**, 151
- Kim J.-h., Lee J., 2013, *MNRAS*, **432**, 1701
- Kormendy J., Ho L. C., 2013, *ARA&A*, **51**, 511
- Kormendy J., Bender R., Cornell M. E., 2011, *Nature*, **469**, 374
- Kroupa P., 2001, *MNRAS*, **322**, 231
- Kumari N., Irwin M. J., James B. L., 2020, *A&A*, **634**, A24
- Le Borgne D., Rocca-Volmerange B., Prugniel P., Lançon A., Fioc M., Soubiran C., 2004, *A&A*, **425**, 881
- Lelli F., Fraternali F., Sancisi R., 2010, *A&A*, **516**, A11
- Lelli F., McGaugh S. S., Schombert J. M., 2016, *ApJ*, **816**, L14
- Lelli F., McGaugh S. S., Schombert J. M., Desmond H., Katz H., 2019, *MNRAS*, **484**, 3267
- Libeskind N. I., Hoffman Y., Tully R. B., Courtois H. M., Pomarède D., Gottlöber S., Steinmetz M., 2015, *MNRAS*, **452**, 1052
- Macciò A. V., Dutton A. A., van den Bosch F. C., Moore B., Potter D., Stadel J., 2007, *MNRAS*, **378**, 55
- Makarov D., Prugniel P., Terekhova N., Courtois H., Vauglin I., 2014, *A&A*, **570**, A13
- Mapelli M., Moore B., Ripamonti E., Mayer L., Colpi M., Giordano L., 2008, *MNRAS*, **383**, 1223
- Martin D. C., et al., 2005, *ApJ*, **619**, L1
- McGaugh S. S., Schombert J. M., 2014, *AJ*, **148**, 77
- McGaugh S. S., Schombert J. M., 2015, *ApJ*, **802**, 18
- McGaugh S. S., Rubin V. C., de Blok W. J. G., 2001, *AJ*, **122**, 2381
- Mishra A., Kantharia N. G., Das M., Omar A., Srivastava D. C., 2017, *MNRAS*, **464**, 2741
- Mo H. J., Mao S., White S. D. M., 1998, *MNRAS*, **295**, 319
- Moore L., Parker Q. A., 2006, *Publ. Astron. Soc. Australia*, **23**, 165
- Müller O., Pawlowski M. S., Jerjen H., Lelli F., 2018, *Science*, **359**, 534
- Naik S., Das M., Jain C., Paul B., 2010, *MNRAS*, **404**, 2056
- Noguchi M., 2001, *MNRAS*, **328**, 353
- Noordermeer E., 2006, PhD thesis, Groningen: Rijksuniversiteit
- Noordermeer E., van der Hulst J. M., 2007, *Monthly Notices of the Royal Astronomical Society*, **376**, 1480
- Noordermeer E., van der Hulst J. M., Sancisi R., Swaters R. S., van Albada T. S., 2007, *Monthly Notices of the Royal Astronomical Society*, **376**, 1513
- Ogle P. M., Lanz L., Nader C., Helou G., 2016, *ApJ*, **817**, 109
- Ogle P. M., Lanz L., Appleton P. N., Helou G., Mazzarella J., 2019, *ApJS*, **243**, 14
- Peñarrubia J., McConnachie A., Babul A., 2006, *ApJ*, **650**, L33
- Pérez-Montaño L. E., Cervantes Sodi B., 2019, *MNRAS*, **490**, 3772
- Pickering T. E., Impey C. D., van Gorkom J. H., Bothun G. D., 1997, *AJ*, **114**, 1858
- Pickering T. E., van Gorkom J. H., Impey C. D., Quillen A. C., 1999, *AJ*, **118**, 765
- Ponomareva A. A., Verheijen M. A. W., Papastergis E., Bosma A., Peletier R. F., 2018, *MNRAS*, **474**, 4366
- Rahman N., Howell J. H., Helou G., Mazzarella J. M., Buckalew B., 2007, *ApJ*, **663**, 908
- Ramya S., Prabhu T. P., Das M., 2011, *MNRAS*, **418**, 789
- Reshetnikov V. P., Moiseev A. V., Sotnikova N. Y., 2010, *MNRAS*, **406**, L90
- Rodríguez-Gomez V., et al., 2015, *MNRAS*, **449**, 49
- Roediger J. C., Courteau S., 2015, *MNRAS*, **452**, 3209
- Roychowdhury S., Huang M.-L., Kauffmann G., Wang J., Chengalur J. N., 2015, *MNRAS*, **449**, 3700
- Saburova A. S., 2018, *MNRAS*, **473**, 3796
- Saburova A. S., Kasparova A. V., Katkov I. Y., 2016a, *MNRAS*, **463**, 2523
- Saburova A. S., Kasparova A. V., Katkov I. Y., 2016b, *MNRAS*, **463**, 2523
- Saburova A. S., Katkov I. Y., Khoperskov S. A., Zasov A. V., Uklein R. I., 2017, *MNRAS*, **470**, 20
- Saburova A. S., Chilingarian I. V., Katkov I. Y., Egorov O. V., Kasparova A. V., Khoperskov S. A., Uklein R. I., Vozyakova O. V., 2018, *MNRAS*, **481**, 3534
- Saburova A., Chilingarian I., Kasparova A., Katkov I., Fabricant D., Uklein R., 2019, arXiv e-prints, p. [arXiv:1908.11383](https://arxiv.org/abs/1908.11383)
- Saha K., Dhiwar S., Barway S., Narayan C., Tandon S. N., 2021, arXiv e-prints, p. [arXiv:2101.07002](https://arxiv.org/abs/2101.07002)
- Sahu N., Graham A. W., Davis B. L., 2019, *ApJ*, **887**, 10
- Salpeter E. E., 1955, *ApJ*, **121**, 161
- Santos-Santos I., et al., 2020, *ApJ*, **897**, 71
- Saulder C., van Kampen E., Chilingarian I. V., Mieske S., Zeilinger W. W., 2016, *A&A*, **596**, A14
- Schombert J., 1998, *AJ*, **116**, 1650
- Schommer R. A., Bothun G. D., 1983, *AJ*, **88**, 577
- Sil'chenko O. K., Burenkov A. N., Vlasjuk V. V., 1998, *New Astronomy*, **3**, 15
- Sil'chenko O. K., Moiseev A. V., Egorov O. V., 2019, *ApJS*, **244**, 6
- Sprayberry D., Bernstein G. M., Impey C. D., Bothun G. D., 1995, *ApJ*, **438**, 72
- Subramanian S., Ramya S., Das M., George K., Sivarani T., Prabhu T. P., 2016, *MNRAS*, **455**, 3148
- Thilker D. A., et al., 2005, *ApJ*, **619**, L79
- Thilker D. A., et al., 2007, *ApJS*, **173**, 538
- Tully R. B., Fisher J. R., 1977, *A&A*, **500**, 105
- Wilman D. J., Fontanot F., De Lucia G., Erwin P., Monaco P., 2013, *MNRAS*, **433**, 2986
- Wyder T. K., et al., 2009, *ApJ*, **696**, 1834
- Yesuf H. M., Faber S. M., Koo D. C., Woo J., Primack J. R., Luo Y., 2020, *ApJ*, **889**, 14
- Yim K., Wong T., Rand R. J., Schinnerer E., 2020, *MNRAS*, **494**, 4558
- Zasov A. V., Khoperskov A. V., Saburova A. S., 2011, *Astronomy Letters*, **37**, 374
- Zasov A., Saburova A., Katkov I., Egorov O., Afanasiev V., 2015, *MNRAS*, **449**, 1605
- Zasov A. V., Saburova A. S., Egorov O. V., Dodonov S. N., 2019, *Monthly Notices of the Royal Astronomical Society*, **486**, 2604
- Zhu Q., et al., 2018, *MNRAS*, **480**, L18
- de Blok W. J. G., McGaugh S. S., Rubin V. C., 2001, *AJ*, **122**, 2396
- de los Reyes M. A. C., Kennicutt Robert C. J., 2019, *ApJ*, **872**, 16
- van Dokkum P. G., Abraham R., Merritt A., Zhang J., Geha M., Conroy C., 2015, *ApJ*, **798**, L45
- van der Kruit P. C., Bosma A., 1978, *Astronomy and Astrophysics*, **70**, 63
- van der Marel R. P., Franx M., 1993, *ApJ*, **407**, 525